RECEIVED
LAWRENCE
RADIATION LABORATORY

DEC 2 1969

LIBRARY AND
DOCUMENTS SECTION

UCRL-19338

NUCLEAR SPINS, $^3P_1$ AND $^3P_2$ HYPERFINE STRUCTURES, AND NUCLEAR MOMENTS OF ^{69}Ge AND ^{75}Ge, AND $^3P_2$ HYPERFINE STRUCTURE OF ^{71}Ge

Abiodun F. Oluwole
(Ph. D. Thesis)

September 10, 1969

AEC Contract No. W-7405-eng-48

TWO-WEEK LOAN COPY

This is a Library Circulating Copy which may be borrowed for two weeks. For a personal retention copy, call Tech. Info. Division, Ext. 5545

LAWRENCE RADIATION LABORATORY
UNIVERSITY of CALIFORNIA BERKELEY

UCRL-19338

DISCLAIMER

This document was prepared as an account of work sponsored by the United States Government. While this document is believed to contain correct information, neither the United States Government nor any agency thereof, nor the Regents of the University of California, nor any of their employees, makes any warranty, express or implied, or assumes any legal responsibility for the accuracy, completeness, or usefulness of any information, apparatus, product, or process disclosed, or represents that its use would not infringe privately owned rights. Reference herein to any specific commercial product, process, or service by its trade name, trademark, manufacturer, or otherwise, does not necessarily constitute or imply its endorsement, recommendation, or favoring by the United States Government or any agency thereof, or the Regents of the University of California. The views and opinions of authors expressed herein do not necessarily state or reflect those of the United States Government or any agency thereof or the Regents of the University of California.

NUCLEAR SPINS, $^3P_1$ AND $^3P_2$ HYPERFINE STRUCTURES, AND NUCLEAR MOMENTS OF ^{69}Ge AND ^{75}Ge, AND $^3P_2$ HYPERFINE STRUCTURE OF ^{71}Ge

Contents

Abstract . . . v

I. Introduction . . . 1

II. Theory . . . 2

A. Atomic Theory . . . 2

B. Hyperfine Structure . . . 5

1. Zero Field . . . 5

2. Addition of an External Field . . . 11

3. Relativistic Corrections to hfs . . . 12

4. Effects of Configuration Interaction . . . 15

C. Nuclear Structure . . . 19

III. Atomic-Beam Magnetic-Resonance Method . . . 26

A. General Description of Apparatus . . . 26

IV. Experiment . . . 33

A. Ge Isotopes . . . 33

B. ^{75}Ge . . . 33

1. Production and Detection . . . 33

2. Beam Formation . . . 35

3. Spin Measurement . . . 37

4. Hyperfine Structure Measurement . . . 41

5. Results . . . 52

C. ^{71}Ge ($^3P_2$) . . . 61

1. Beam Formation . . . 62

2. Results and Discussion . . . 62

D. ^{69}Ge ($^3P_1$) 63

1. Production 63

2. Beam Formation 69

3. Spin Measurement 70

4. Hyperfine Structure Measurement 72

5. Results and Interpretations 80

Acknowledgments 88

Appendices 89

References 93

NUCLEAR SPINS, $^3P_1$ AND $^3P_2$ HYPERFINE STRUCTURES, AND NUCLEAR MOMENTS OF ^{69}Ge AND ^{75}Ge, AND $^3P_2$ HYPERFINE STRUCTURE OF ^{71}Ge

Abiodun F. Oluwole

Department of Physics and Lawrence Radiation Laboratory
University of California
Berkeley, California

September 10, 1969

ABSTRACT

The atomic-beam magnetic-resonance (ABMR) technique has been used to measure the nuclear spin, I, and the $^3P_1$ hyperfine structure (hfs) constants, a and b, for 37-hr ^{69}Ge, the $^3P_2$ hfs constant a for 11-day ^{71}Ge, and the nuclear spin and hfs constant a for ^{75}Ge in the $^3P_1$ and $^3P_2$ electronic states. The nuclear moments were inferred by the use of the Fermi-Segrè formula from the corresponding hfs interaction constants.

The results are:

Isotope	Spin	hfs constants	Moments (uncorr.)	χ^2
^{69}Ge	I=5/2	$a(^3P_1) = \pm 23.39(5)$ MHz	$\mu_I = \mp 0.733(7)$ nm	7.97
		$b(^3P_1) = \mp 8.28(8)$ MHz	$Q_I = \mp 0.043(8)$ barns	
^{71}Ge	I=1/2 (prev. meas.)	$a(^3P_2) = +360.54(6)$ MHz		0.56
^{75}Ge	I=1/2	$a(^3P_1) = -81.05(8)$ MHz	$\mu_I = +0.509(5)$ nm	2.28
		$a(^3P_2) = +335.94(9)$ MHz		0.55

The figures in parentheses represent the error in the last figure. For the hfs constants this is two standard deviations. A 1% uncertainty is given for the magnetic moment to include a possible hfs anomaly. The 20% error for Q results from the theoretical problem of extracting Q from b.

Relativistic effects account for about 25% of the a values while the remainder is attributed to effects of configuration interaction. The nuclear spins are predicted correctly by the shell model, while the quasi-particle nuclear theory of Migdal is found to predict the nuclear moments more accurately than the shell model.

I. INTRODUCTION

This research is part of a continuing program by the Atomic Beam Group of the Lawrence Radiation Laboratory to measure nuclear spins and electromagnetic moments of radioactive atoms.

Measurements of the hfs interaction constants of germanium isotopes are of interest because of the light they shed on the electronic structure of the germanium atom. This is especially so in the $^3P_1$ electronic state where the magnetic dipole interaction constant must vanish except for contributions due to relativistic effects and configuration interaction.

In the first part of this thesis, relevant atomic and nuclear theories are discussed. A description of the apparatus and experimental techniques associated with the ABMR method is given. Our results are then listed and the observed values are compared with those predicted theoretically. Most of these results have been published in abstract form.[1]

II. THEORY

A. Atomic Theory

The non-relativistic Hamiltonian for a free atom with a nuclear charge Ze can be written as[2]

$$\mathcal{H} = \sum_i \left(\frac{\hbar^2}{2m_i} \nabla_i^2 - \frac{Ze^2}{r_i} \right) + \sum_{i<j} \frac{e^2}{r_{ij}} + \sum_i \xi_i(r_i) \vec{\ell}_i \cdot \vec{s}_i + \mathcal{H}_{hfs} \qquad (1)$$

where r_i is the distance of the ith electron from the nucleus and r_{ij} the distance between the ith and j^{th} electron.

The first term in the Hamiltonian is the sum of the kinetic energies in the field of the nucleus. The second term is the repulsive Coulomb potential energy between pairs of electrons. The third term represents the interaction of the electron's spin with the magnetic field produced by its orbital motion in the Coulomb field of the nucleus. The last term is the hfs interaction energy. The last term is much smaller than the others and will receive a separate treatment in the next section. Here we shall mainly concern ourselves with the first three terms.

Since an exact solution of this Hamiltonian is at present not possible, we use the perturbation approach. The Central Field Approximation is a convenient starting point for obtaining the energy levels. In this approximation, each electron moves independently in the field of the nucleus and interacts with a central field expressed by the spherically symmetric potential U(r). The Schrödinger Equation is then

$$\mathcal{H}_{cf}\psi_{cf} = \left[\sum_i \left(\frac{\hbar^2}{2m_i} \nabla_i^2 + U_i(r_i) \right) \right] \psi_{cf} = E_{cf}\psi_{cf} \quad . \qquad (2)$$

The difference in the Hamiltonians represented by Eq. (1) and (2) is then treated as perturbation potential V where

$$V = \mathcal{H} - \mathcal{H}_{cf} = \sum_{i=1}^{Z}\left(-\frac{Ze^2}{r_i} - U(r_i)\right) + \sum_{i<j}\frac{e^2}{r_{ij}} + \sum \xi_i(r_i)\vec{\ell}_i\cdot\vec{s}_i \quad . \tag{3}$$

The eigenstates of $\mathcal{H}_{cf}$ are products of single electron wave-functions.

$$\psi_{cf} = \prod_i \phi_i(r_i) \;\; ; \;\; E_{cf} = \sum_i E_i \tag{4}$$

where

$$\left(-\frac{\hbar^2}{2m}\nabla^2 + U(r)\right)\phi_i = E_i\phi_i \quad . \tag{5}$$

A further separation of variables is possible by introducing polar coordinates

$$\phi_i(a_i) = r^{-1}R_{n\ell}(r)\; Y^{\ell}_{m_\ell}(\theta,\phi) \tag{6}$$

where (a_i) represents a set of quantum numbers $(n\ell m_\ell)$ which specify the state of motion of the single electron in the Central Field.

We can then take the spin of the electron into consideration by including in each ϕ_i a factor α or β, corresponding to $m_s = +1/2$ or $m_s = -1/2$.

Then

$$\phi(\alpha_i) = r^{-1}R_{n\ell}(r)\, Y^{\ell}_{m_\ell}(\theta,\phi)\left\{\begin{matrix}\alpha\\ \beta\end{matrix}\right\} \tag{7}$$

where α_i represents the quantum numbers (n,ℓ,m_ℓ,m_s); also

$$\psi_{cf} = \prod_i \phi(\alpha_i) \quad . \tag{8}$$

The product wave function satisfying the Pauli Exclusion Principle is given by the Slater determinant:

$$\psi = \frac{1}{\sqrt{N!}} \begin{vmatrix} \phi_1(\alpha_1) & \phi_2(\alpha_1) & \cdots & \phi_N(\alpha_1) \\ \vdots & & & \\ \phi_1(\alpha_N) & \phi_2(\alpha_N) & \cdots & \phi_N(\alpha_N) \end{vmatrix} . \tag{9}$$

The energy eigenvalues correspond to the energy of a particular electronic configuration which is described in terms of the quantum numbers

$$(n_1\ell_1)^{K_1} (n_2\ell_2)^{K_2} \cdots (n_N\ell_N)^{K_N}$$

where K_1 represents the number of times $(n_1\ell_1)$ occurs.

The effects of the perturbation potential V on the above energy levels will now be discussed. Recall that

$$V = \sum_{i=1}^{Z} \left[- \frac{Ze^2}{r_i} - U(r_i) \right] + \sum_{i<j} \frac{e^2}{r_{ij}} + \sum_i \xi_i(r_i) \vec{\ell}_i \cdot \vec{s}_i \quad .$$

The first term is purely radial and merely contributes equal energy shifts to all the levels belonging to a given configuration. The last two terms are different for different states of the same configuration. We may therefore treat as our new perturbation V'

$$V' = \sum_{i<j} \frac{e^2}{r_{ij}} + \sum_i \xi_i(r_i) \vec{\ell}_i \cdot \vec{s}_i \quad . \tag{10}$$

Two distinct cases obtain for the perturbation V' depending on the relative strengths of the electrostatic repulsion term and the spin-orbit term. First, if $(e^2/r_{ij}) >> [\xi_i(r_i)\vec{\ell}_i \cdot \vec{s}_i]$, one can use the LS coupling scheme. If we define $\vec{L} = \sum_i \ell_i$ and $\vec{S} = \sum_i s_i$, then $\vec{L}$ and $\vec{S}$ commute with $\sum \frac{e^2}{r_{ij}}$, and L and S are good quantum numbers. They are used to specify the energy levels produced by the $\sum \frac{e^2}{r_{ij}}$ term. These levels are labelled ^{2S+1}L. They are (2S+1)(2L+1)-fold degenerate. The spin-

orbit term does not commute with either L or S but does commute with $\vec{J} = \vec{L} + \vec{S}$. Hence it splits each term into multiplets labelled $^{2S+1}L_J$. Each multiplet is 2J+1 degenerate.

On the other hand, if $(e^2/r_{ij}) << [\xi_i(r_i)\vec{\ell}_i \cdot \vec{s}_i]$, then one has to employ the j-j coupling scheme. For each electron, $\vec{\ell}_i$ and $\vec{s}_i$ are coupled to angular momentum $\vec{j}_i = \vec{\ell}_i + \vec{s}_i$, and the resultant total angular momentum is $\vec{J} = \sum j_i$. J is a good quantum number. By arguments parallel to those above, one arrives at a set of 2J+1 degenerate levels.

This perturbation approach is illustrated diagrammatically in Fig. 1.

B. Hyperfine Structure

1. Zero Field

The Hamiltonian, $\mathcal{H}_{cf}$, treated in the last section, yields energy levels which are (2J+1)-fold degenerate. This degeneracy can be removed not only by an external field but also by the non-spherically-symmetric interaction of the electrons with the nucleus.[3]

The kinds of interaction are limited by parity considerations. In general, nuclei may have only odd magnetic moments and even electric moments.

Schwartz[4] has shown that hfs Hamiltonian can be written in tensor form:

$$\mathcal{H}_{hfs} = \sum_{i=1}^{\infty} T_e^{(i)} \cdot T_n^{(i)} \quad .$$

Using group-theoretical arguments, it can be shown that the largest multipole interaction is of order 2^{ℓ}, where $\ell = \min(2J,2I)$. By far the

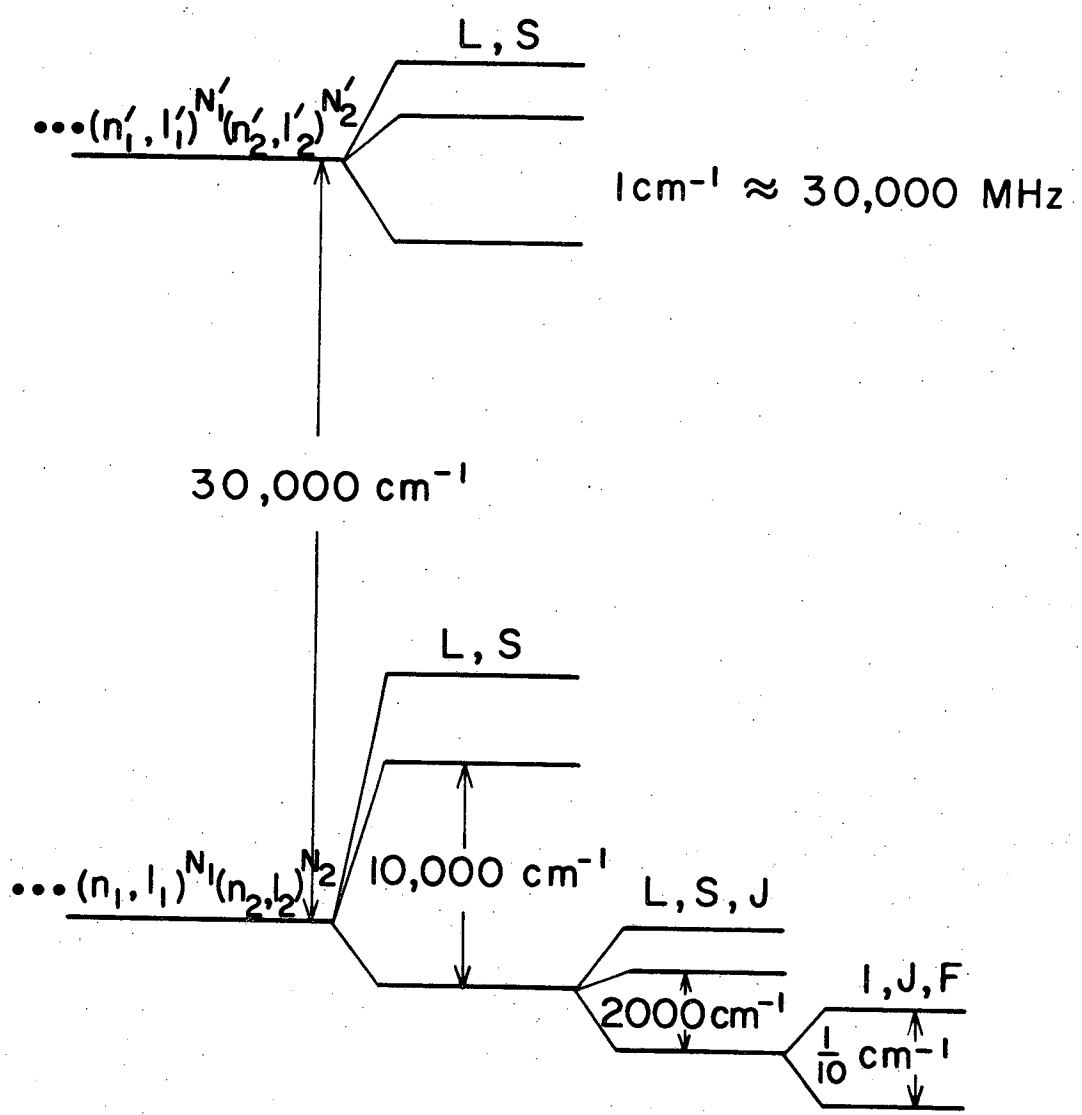

XBL674-2780

Fig. 1. The Russell-Saunders coupling scheme, showing the usual quantum numbers and typical energy separations.

largest contributions come from the nuclear magnetic moment and the electric quadrupole moment interactions.

The $\mathcal{H}_{hfs}$ is then[5]

$$\mathcal{H}_{hfs} = -\sum_{i=1}^{N} \vec{H}_i \cdot \vec{\mu} - e^2 \int_{\tau_e} \int_{\tau_n} \frac{\rho_e(r_e)\rho_n(r_n)}{|\vec{r}_e - \vec{r}_n|} d\tau_e d\tau_n - Ze \int_{\tau_e} d\tau_e \frac{\rho_e}{r_e}$$

$$= \mathcal{H}_m + \mathcal{H}_E \quad . \tag{11}$$

$\mathcal{H}_m$ is the energy of interaction between the magnetic field H_i of each electron and the nuclear moment μ. $\mathcal{H}_E$ is the electrostatic interaction between the charged nucleus and electrons.

The magnetic field H_i, of an orbital electron,[3] is

$$\vec{H}_i = \frac{e(\vec{v}_i \times \vec{r}_i)}{r^3} + \frac{\vec{\mu} r_i^2 - 3\vec{r}_i(\vec{\mu}\cdot\vec{r}_i)}{r^5}$$

$$= 2\beta \frac{\vec{\ell}_i - \vec{s}_i}{r^3} + \frac{3\vec{r}_i(\vec{s}_i \cdot \vec{r}_i)}{r^5} \tag{12}$$

where

$$2\beta\vec{S} = \vec{\mu} \quad .$$

Hence

$$\mathcal{H}_m = 2\beta\ \beta_N\ g_I \sum_i \frac{\vec{N}_i \cdot \vec{I}}{r_i^3} \tag{13}$$

and

$$\vec{N}_i = \vec{\ell}_i - \vec{s}_i + \frac{3\vec{r}_i}{r^2}(\vec{s}_i \cdot \vec{r}_i) \quad .$$

We can put $\vec{N}_i$ in a tensorial form[6]

$$\vec{N}_i = \vec{\ell}_i - (10)^{1/2}\ (\vec{s}\vec{C}^{(2)})_i^{(1)}$$

and then write

$$\mathcal{H}_m = a_\ell \sum_i [\vec{\ell}_i - (10)^{1/2}\ (\vec{s}\vec{C}^{(2)})_i^{(1)}] \cdot \vec{I} \tag{14}$$

with

$$a_\ell = 2\beta\ \beta_N\ g_I\ \langle r^{-3}\rangle = 2\beta\ \beta_N \frac{\mu_I}{I} \langle r^{-3}\rangle \quad . \tag{14a}$$

In the absence of an external field, I and J are strongly coupled to form states of total angular momentum $\vec{F} = \vec{I} + \vec{J}$. In this state the characteristic quantum numbers are $|IJFM_F\rangle$.

We then calculate the matrix elements of $\mathcal{H}_m$ in the $|IJFM_F\rangle$ scheme. They can be written as

$$\langle \alpha IJFM|\mathcal{H}_m|\alpha' IJFM\rangle = (-1)^{J+I+F}\ a_\ell \begin{Bmatrix} J & J & 1 \\ I & I & F \end{Bmatrix} \langle I\|I^{(1)}\|I\rangle \times \langle \alpha J\|\Sigma\vec{N}_i\|\alpha J\rangle . \tag{15}$$

By writing out the 6-j symbol, Eq. (15) reduces to

$$\langle |\mathcal{H}_m|\rangle = \frac{a_\ell K}{2} \frac{\langle \alpha J\|\Sigma\vec{N}_i\|\alpha' J\rangle}{[J(J+1)(2J+1)]^{1/2}}$$

$$= \frac{1}{2}\ aK \tag{16}$$

where

$$K = F(F+1) - J(J+1) - I(I+1) \tag{17}$$

and

$$a = a_\ell \frac{\langle \alpha J\|\Sigma\vec{N}_i\|\alpha' J\rangle}{[J(J+1)(2J+1)]^{1/2}} \quad . \tag{18}$$

a is known as the magnetic hfs constant and can be experimentally determined.

Equation (18) can be further simplified for the Hund's Rule ground state of an $(\ell)^N$ configuration. This is the state with maximum L and S consistent with the Exclusion Principle[7] – $\ell^n\ {}^{2S+1}L_J$. In this case

$$a = a_\ell \Bigg[2 - g + \frac{2(2L - n^2)}{n^2(2L-1)(2\ell-1)(2\ell+3)} \Bigg\{ \frac{L(L+1)}{2J(J+1)} [J(J+1) + S(S+1) - L(L+1)]$$
$$- \frac{3}{4} \frac{[J(J+1) - L(L+1) - S(S+1)][J(J+1) + L(L+1) - S(S+1)]}{J(J+1)} \Bigg\} \Bigg] \quad . \tag{19}$$

From Eq. (16) we see that $\mathcal{H}_m$ can also be written in a handier fashion:

$$\mathcal{H}_m = a\vec{I}\cdot\vec{J} \quad . \tag{20}$$

A similar explicit expression is now sought for the matrix elements of $\mathcal{H}_E$:

$$\mathcal{H}_E = -e^2\int_{\tau_e}\int_{\tau_n} \frac{\rho_e(r_e)\rho_n(r_n)}{|\vec{r}_e - \vec{r}_n|}\, d\tau_e d\tau_n + Ze\int_{\tau_e} d\tau_e \frac{\rho_e}{r_e} \quad .$$

$\frac{1}{|\vec{r}_e-\vec{r}_n|}$ can be expanded in spherical harmonics:

$$\frac{1}{|\vec{r}_e-\vec{r}_n|} = \sum_k \frac{r_n^k}{r_e^{k+1}} (\vec{C}_e^{(k)}\cdot\vec{C}_e^{(k)}) \quad . \tag{21}$$

Since $\mathcal{H}_E$ must be invariant under inversion of coordinates, parity considerations rule out the k-odd terms. The k=0 term is the Coulomb term which cancels the second term. The k=2 term is the electric quadrupole interaction. Higher terms make contributions which are much smaller than the present limit of observation and will therefore be neglected.

Then

$$\mathcal{H}_E = e^2\int_{\tau_n}\int_{\tau_e} \rho(r_e)\rho(r_n)\, \frac{r_n^2}{r_e^3}\, (\vec{C}_n^{(2)}\cdot\vec{C}_e^{(2)})\, d\tau_e d\tau_n \quad . \tag{22}$$

Following Casimir[8] and Wybourne[5] we write out the matrix elements of $\mathcal{H}_E$ in the $|IJFM_F\rangle$ scheme:

$$\langle\alpha IJFM_F|\mathcal{H}_E|\alpha' IJFM_F\rangle = -(-1)^{J+I+F}\, e^2 \begin{Bmatrix} J & J & 2 \\ I & I & F \end{Bmatrix} \langle\alpha J\|r_e^{-3}\, \vec{C}_e^{(2)}\|\alpha' J\rangle \times \langle I\|r_n^2\, \vec{C}_n^{(2)}\|I\rangle . \tag{23}$$

The quadrupole moment is defined as

$$Q = (II|r_n^2\vec{C}_n^{(2)}|II) \tag{24}$$

$$= \begin{pmatrix} I & 2 & I \\ -I & 0 & I \end{pmatrix} (I\|r_n^2\vec{C}_n^{(2)}\|I) \quad .$$

On evaluating the 3-j symbol, we obtain

$$Q = \left(\frac{2I(2I-1)}{(I+1)(2I+1)(2I+3)}\right)^{1/2} (I\|r_n^2\vec{C}_n^{(2)}\|I) \quad .$$

Thus Eq. (23) becomes

$$\langle|\mathcal{H}_E|\rangle = b_\ell X_J \frac{\frac{3}{2}K(K+1) - I(I+1)J(J+1)}{2I(2I-1)J(2J-1)} \tag{25}$$

where

$$b_\ell = e^2Q\langle r^{-3}\rangle$$

$$X_J = \frac{4J(2J-1)}{(J+1)(2J+1)(2J+3)} \langle\alpha J|\vec{C}_e^{(2)}|\alpha' J\rangle \quad .$$

The gradient of the electric field enters into the expression $\langle\alpha J|\vec{C}_e^{(2)}|\alpha' J\rangle$ of the X_J term.

The electric quadrupole hfs interaction constant b is usually defined as

$$b = b_\ell X_J \quad . \tag{26}$$

Finally, in the absence of external fields, the matrix elements for $\mathcal{H}_{hfs}$ may be written

$$\begin{aligned}\langle\alpha IJFM_F|\mathcal{H}_{hfs}|\rangle &= \langle|\mathcal{H}_m|\rangle + \langle|\mathcal{H}_E|\rangle \\ &= \frac{aK}{2} + b\frac{\frac{3}{4}K(K+1) - I(I+1)J(J+1)}{2I(2I-1)J(2J-1)} \quad .\end{aligned} \tag{27}$$

We note that both a and b contain an $\langle r^{-3}\rangle$ term. This means we cannot extract nuclear moments from experimentally measured quantities a and b without knowing the electronic wave functions. However, if the nuclear parameters for one isotope are independently determined, the Fermi-Segrè formula derived from Eq. (14a)

$$\left(\frac{a}{g_I}\right)_1 = \left(\frac{a}{g_I}\right)_2 (1 + {}^1\Delta^2) \tag{28}$$

may be used to compare the isotopes,[9] where g_I is the nuclear g-factor and ${}^1\Delta^2$ is the hfs anomaly for the two isotopes. The anomaly is

usually less than 1% or negligible for non-s electrons. $\langle r^{-3}\rangle$ may also be extracted from the spin orbit interaction constant ξ:

$$\langle r^{-3}\rangle = \frac{\xi}{2\mu_o^2 Z_{eff} H} \quad . \tag{29}$$

The value of $\langle r^{-3}\rangle$ obtained by the latter method usually differs from that calculated from hfs constant a.

2. Addition of an External Field

The hfs interaction levels are (2F+1)-fold degenerate. The addition of an external field removes this degeneracy.

The Hamiltonian in the external magnetic field, H_o, is

$$\mathcal{H}' = \mathcal{H}_{hfs} - g_I \mu_o \vec{I}\cdot\vec{H}_o - g_J \mu_o \vec{J}\cdot\vec{H}_o \quad . \tag{30}$$

At low fields I and J are strongly coupled to $\vec{F} = \vec{I} + \vec{J}$. The matrix elements are evaluated in the $|IJFM\rangle$ representation

$$\langle IJFM|\mathcal{H}'|IJFM\rangle = \langle|\mathcal{H}_{hfs}|\rangle - g_F \mu_o M_F H_o \quad , \tag{31}$$

where $\langle|\mathcal{H}_{hfs}|\rangle$ is given by Eq. (27), and

$$g_F = g_J \frac{F(F+1)+J(J+1)-I(I+1)}{2F(F+1)} + g_I \frac{F(F+1)+I(I+1)-J(J+1)}{2F(F+1)} \quad . \tag{32}$$

At high fields, where I and J are completely decoupled, the $|IM_I JM_J M_F\rangle$ representation is used to calculate matrix elements. F is no longer a good quantum number, but M_F remains a good one in both representations.

At intermediate values of the field H_o, the matrix elements are no longer diagonal in either representation. It is necessary to compute the matrix elements of $\mathcal{H}'$ in either scheme and diagonalize the resulting matrix.

A special case arises when either I or J = 1/2. Then the diagon-

alization can be solved in a closed form. Since $\mathcal{H}'$ is diagonal in M_F, the matrix breaks up into a series of 2x2 blocks along the diagonal, each corresponding to a value of $M_F = M_I + M_J$. In the $|IJFM_F\rangle$ representation it has the form (when I = 1/2)

$$\begin{array}{c|cc} & F = J+\frac{1}{2} & F = J-\frac{1}{2} \\ \hline F = J+\frac{1}{2} & a\frac{J}{2} - \frac{\mu_o H_o M_F}{(2J+1)}(2g_J J+g_I) & -\mu_o H_o (g_J-g_I)[(J+\frac{1}{2})^2 - M_F^2]^{1/2} \\ F = J-\frac{1}{2} & \frac{\mu_o H_o (g_J-g_I)}{(2J+1)}[(J+\frac{1}{2})^2-M_F^2]^{1/2} & -\frac{a}{2}(J+1) - \frac{\mu_o M_F H_o}{(2J+1)}[2g_J(J+1)-g_I] \end{array} .$$

The quadratic equation which results can be solved to yield the Breit-Rabi formula[10] for the energy $W_\pm$

$$W_\pm = -\frac{h\Delta\nu}{2(2J+1)} - g_J\mu_o H_o M_F \pm \frac{h\Delta\nu}{2}\left[1 + \frac{4M_F x}{(2J+1)} + x^2\right]^{1/2} \qquad (33)$$

where

$$\Delta\nu = a(J + 1/2) \quad ;$$

$$x = \frac{(g_J - g_I)\mu_o H_o}{h\Delta\nu} .$$

W_+ and W_- respectively refer to states with F = J+1/2 and F = J-1/2. The electric-quadrupole term identically vanishes since I < 1.[3]

Since two of the isotopes under consideration (^{71}Ge and ^{75}Ge) have each a spin of I = 1/2, Eq. (33) will completely describe their hfs.

For the general case, when I,J > 1/2, one has to resort to numerical methods and the computer for a solution of the eigenvalue equation.[11]

3. Relativistic Corrections to hfs

It is always necessary to know the radial part of the hfs constants a_ℓ and b_ℓ in order to deduce the values of nuclear moments from them.

Relativistic modifications of these radial parts can be considerable.

Many authors[8,12,13] have considered this problem extensively. Expressions have been derived for relativistic corrections to hfs constants. Here we shall sketch a method for obtaining the Casimir corrections to hfs constants.

The relativistic treatment of hfs starts with the consideration of a single electron in a central field. The electron wave function obeys the Dirac Equation:

$$[\vec{\alpha}\cdot(c\vec{p} + e\vec{A}) + \vec{\beta}(mc^2 - eV)]\psi = E\psi \quad . \tag{34}$$

The four-component wave function ψ is formed from anti-symmetric products of single-particle functions of the form[8]

$$\psi_j(r,\theta,\phi) = U^R_{n_\ell jm} = \begin{pmatrix} \Theta_{\ell jm} & \frac{g(r)}{r} \\ \Theta_{\ell jm} & \frac{if(r)}{r} \end{pmatrix} \tag{35}$$

where

$$\Theta_{\ell jm} = \sum_\sigma \langle \tfrac{1}{2}\ell jm | 1/2 | \sigma m-\sigma \rangle \phi^\sigma Y_{\ell m-\sigma} \quad .$$

$Y_{\ell m-\sigma}$ is a spherical harmonic, ϕ^σ is the spin function with $S_Z = \sigma$, and $\langle \frac{1}{2}\ell jm | 1/2 | \sigma m-\sigma \rangle$ is the Clebsch-Gordan coefficient. $g(r)$ and $f(r)$ are radial wavefunctions, and in the non-relativistic case $g(r)$ is finite while $f(r) \to 0$.

The central problem is the evaluation of the radial integrals associated with the magnetic dipole and electric quadrupole interactions.

The solution of Dirac's Equation for small r (this is where relativistic effects are pronounced) is first considered.

We put $\chi_1 = rf(r)$ and $\chi_2 = rg(r)$. (36)

Then

$$\frac{d\chi_1}{dr} + \frac{k\chi_1}{r} = -\frac{2\alpha}{r}\chi_2$$

$$\frac{d\chi_2}{dr} - \frac{k\chi_2}{r} = (2 + \frac{Z\alpha}{r})\chi_1 \tag{37}$$

where

$$k = \ell + 1 \quad \text{for} \quad J = \ell + 1/2$$

$$= -\ell \quad \text{for} \quad J = \ell - 1/2 \quad .$$

Equation (37) is solved in terms of Bessel's functions to give

$$\chi_1 = C\alpha Z J_{2\rho}(x)$$

$$\chi_2 = \frac{C}{2}[xJ_{2\rho+1}(x) - 2(\rho+k)J_{2\rho}(x)] \tag{38}$$

where

$$x = (8Z\alpha r)^{1/2} \quad \text{and} \quad \rho = (k^2 - Z^2\alpha^2)^{1/2} \quad .$$

The normalization constant C has been evaluated in terms of the fine structure separation ξ of the states $J = \ell + 1/2$ and $J = \ell - 1/2$. Denoting these states respectively by single and double prime,

$$C^2 = \frac{\alpha\xi}{4Z(\rho' - \rho'' - 1)} \quad . \tag{39}$$

Following Casimir, we define

$$H(\ell, Z_i) = \frac{2\ell(\ell+1)(\rho'-\rho''-1)}{\alpha^2 Z^2} \tag{40}$$

$$F_r(J,Z) = \frac{2J(J+1)(2J+1)}{(4\rho^2-1)} \tag{41}$$

$$R_r(J,Z) = (\ell+1)(2\ell+1)\frac{3k(k+1)-\rho^2+1}{\rho(\rho^2-1)(4\rho^2-1)} \quad . \tag{42}$$

For the magnetic dipole integral[8] he obtained

$$\int_0^\infty r^{-2}\chi_1\chi_2 dr = \frac{-2\alpha C^2 Z^2 F_r(J,Z)}{a(2\ell+1)[\pm(2\ell+1)+1]} \quad . \tag{43}$$

The ± sign in the denominator stands for $J = \ell \pm 1/2$. For the electric-quadrupole, the integral is

$$\int_0^\infty r^{-3}(\chi_1^2 + \chi_2^2)dr = \frac{2\alpha^2 C^2 Z^2 R_r(J,Z)}{a^2[\ell(\ell+1)(2\ell+1)]} \quad . \tag{44}$$

The relativistic expression for hfs constant a becomes

$$a_J = a_{\ell\pm 1/2} = a_{n\ell}\,\frac{\ell(\ell+1)}{J(J+1)}\,F_r(J,Z) \tag{45}$$

where

$$a_{n\ell} = 2\beta\,\beta_N g_I \langle r^{-3}\rangle$$

and

$$\langle r^{-3}\rangle = \frac{\xi}{\beta^2(2\ell+1)Z_i H_r(\ell,Z_i)} \quad . \tag{46}$$

The electric-quadrupole hfs constant is given by

$$b_J = e^2 Q \frac{2J+1}{2J+2}\langle r^{-3}\rangle R_r(J,Z) \quad . \tag{47}$$

The numerical values of the relativistic correction factors $F_r(J,Z)$, $R_r(J,Z)$, and $H_r(\ell,Z_i)$ are tabulated by Kopfermann.[12]

4. Effects of Configuration Interaction

Usually configurations that differ by the excitation of a single electron produce interactions that significantly affect the hfs constants. This is so because the hfs interaction operators are essentially all one-electron operators. These effects are more pronounced in the quadrupole constant than in the corresponding hfs magnetic-dipole constant.

Several authors have attempted to derive expressions for the effect, but none can claim any exactness close to what the present experimental observations demand.

Rajnak and Wybourne,[14] using second-order perturbation theory,

have derived expressions for the corrections due to the effect of closed-shell excitations on the hfs matrix elements:

$$\langle n\ell^N \alpha SLJ | \mathcal{H}_{hfs} | n\ell^N \alpha' S'L'J' \rangle \quad .$$

Their calculations indicate that the quadrupole matrix element is multiplied by a factor $1-\gamma_q$ where

$$\gamma_q = \frac{2(\ell'\|\vec{C}^{(2)}\|\ell'')\langle n'\ell'|r^{-3}|n\ell'\rangle}{\Delta E(\ell\|\vec{C}^{(2)}\|\ell)\langle n\ell|r^{-3}|n\ell\rangle}$$

$$\times \frac{2}{5}\chi\ (2,\ell''\ell,\ell'\ell) - \sum(-1)^k \begin{Bmatrix} \ell' & \ell'' & 2 \\ \ell & \ell & k \end{Bmatrix} \times \chi(k,\ell\ell'',\ell\ell') \qquad (48)$$

where

$$\chi(k,ab,cd) = (a\|\vec{C}^{(k)}\|c)(b\|\vec{C}^{(k)}\|a)R^k(ab,cd)$$

and $R^k(ab,cd)$ is a Slater integral.

What is important here is to note that the electric quadrupole constant b is merely multiplied by a scaling factor. The quadrupole moment is increased or decreased according to whether $\gamma_q < 1$ or $\gamma_q > 1$.

Also, for two states of the same configuration:

$$\frac{b_1(1-\gamma_q)}{b_2(1-\gamma_q)} = \frac{Q_1}{Q_2} = \frac{b_1}{b_2} \quad .$$

The corrections are similar to the ones calculated by Sternheimer.[15]

For the magnetic dipole case, the hfs constant is better written as (see Eq. (19)):

$$a = a_\ell(L + S) \qquad (49)$$

where $L = 2-g$ represents the interactions of the electron orbital motion with the nuclear magnetic moment, and S represents the interactions of the electron spin moments with the nuclear magnetic moment. Configuration mixing introduces scaling factors $(1-\gamma_m)$ and $(1-\gamma_{m'})$ to

both L and S.

Equation (19) is then replaced by

$$a = a_\ell[L(1-\gamma_m) + S(1-\gamma_{m'})] \quad . \tag{50}$$

Both γ_m and $\gamma_{m'}$ are given in Ref. 14. For two states of the same configuration:

$$\frac{a_1}{a_2} = \frac{L_1(1-\gamma_m) + S_1(1-\gamma_{m'})}{L_2(1-\gamma_m) + S_2(1-\gamma_{m'})} \tag{51}$$

$$\neq \frac{L_1 + S_1}{L_2 + S_2} \quad .$$

Hence configurations effects are not just a scaling factor for the total hfs constant a. To calculate completely the values of γ_m and $\gamma_{m'}$, the a values for at least three states of the same configuration must be known.

Another way of looking at the problem is to associate a magnetic field $\vec{H}_{cp}$ at the nucleus with the effect of the electron excited from the core, thereby polarizing the core.[16]

This field has the vector properties of the spin

$$\vec{H}_{cp} = C\vec{S} \quad . \tag{52}$$

The interaction of this field with the nuclear moment gives

$$W_{cp} = \vec{\mu}_N \cdot \vec{H}_{cp} = C'\vec{I}\cdot\vec{S} \tag{53}$$

$$\vec{I}\cdot\vec{S} = \frac{(\vec{I}\cdot\vec{J})(\vec{J}\cdot\vec{S})}{J(J+1)} \quad .$$

In the ^3P states (Ge ground state), (S) = (L). Hence

$$\vec{J}\cdot\vec{S} = \frac{1}{2}J(J+1)$$

$$\therefore \quad W_{cp} = C''\vec{I}\cdot\vec{J} \tag{54}$$

The contribution, therefore, from this effect to the hfs interaction energy, is a constant added to a, the hfs constant; because in this special case (^3P states), C″ is independent of J.

a. Sandars' Method. Very recently Sandars and Beck[13] have developed a theory that enables one to do hfs relativistic calculations for many-electron atoms. This is achieved by developing some effective operators that reproduce the relativistic effects. The matrix elements of these operators between LS wavefunctions yield the correct relativistic expressions. These effective operators are of the form

$$\mathcal{H}^k_{\text{hfs eff.}} = T^{(k)}_n \cdot T^{(k)}_{\text{eff.}} \tag{54a}$$

where

$$T^{(k)}_{\text{eff.}} = \sum_{k_s k_\ell} P^{(k_s k_\ell)k} \, U^{(k_s k_\ell)k} \quad . \tag{54b}$$

$P^{(k_s k_\ell)k}$ are coefficients involving radial integrals of the Casimir type. They are listed in the Appendices. $U^{(k_s k_\ell)k}$ are tensors of rank k_s in spin space, k_ℓ in orbital space, and k in combined spin-orbital space. They have the property that

$$\langle \tfrac{1}{2}\ell \| U^{(k_s k_\ell)} \| \tfrac{1}{2}\ell \rangle = 1 \quad . \tag{54c}$$

For the magnetic dipole case, k_s is restricted to 0, or 1. Hence $T^{(1)}_{\text{eff.}}$ contains three terms: $U^{(01)1}$, $U^{(12)1}$, and $U^{(10)1}$. Sandars and Beck[13] have shown that these are respectively proportional to $\vec{\ell}$, $(\vec{s}\vec{C}^{(2)})^{(1)}$, and $\vec{s}$. The hfs Hamiltonian is then written as

$$\mathcal{H}^1_{\text{hfs eff.}} = 2\mu_0 \frac{\mu_I}{I} \vec{I} \cdot \sum \{ \vec{\ell} \langle r^{-3} \rangle_{01} - (10)^{1/2} (\vec{s}\vec{C}^{(2)})^{(1)} \langle r^{-3} \rangle_{12} + \vec{s} \langle r^{-3} \rangle_{10} \} \quad . \tag{54d}$$

The $\langle r^{-3} \rangle$ expressions are relativistic integrals, listed in the Appendices.

The above expression is essentially the same as the non-relativistic one given by Eq. (14), except for the presence of the last term. In the non-relativistic case $\langle r^{-3}\rangle_{10} = 0$.

b. J-Mixing Corrections to hfs. It is known that $\mathcal{H}_{hfs}$ mixes electronic states of different J. For the general matrix element $\langle IJF|\mathcal{H}_{hfs}|IJ'F\rangle$, the dipole moment operator mixes states with $\Delta J = 0,\pm1$, whereas the quadrupole moment operator mixes states differing by $\Delta J = 0,\pm1,\pm2$.

Woodgate[33] has considered second-order corrections δE_{hfs} to the hfs energy, where

$$\delta E_{hfs} = \frac{\sum_{J'} \langle IJF|\mathcal{H}_{hfs}|IJ'F\rangle\langle IJ'F|\mathcal{H}_{hfs}|IJF\rangle}{E_J - E_{J'}} \tag{54e}$$

and $E_J - E_{J'}$ equals the energy separation of the F-level in states J and J'. For corrections to a, he obtained

$$\delta a(J) = \frac{\delta A_1(J)}{IJ} \tag{54f}$$

where

$$\delta A_1(J) = \begin{pmatrix} I & 1 & I \\ -I & 0 & I \end{pmatrix}\begin{pmatrix} J & 1 & J \\ -J & 0 & J \end{pmatrix}\langle I\|x^{(1)}(n)\|I\rangle\langle J\|x^{(1)}(e)\|J\rangle \ , \tag{54g}$$

and

$$\langle I\|x^{(1)}(n)\|I\rangle\langle J\|x^{(1)}(e)\|J\rangle = (-1)^{2I+2J+3} \begin{Bmatrix} 1 & 1 & 1 \\ I & I & I \end{Bmatrix}\begin{Bmatrix} 1 & 1 & 1 \\ J & J & J \end{Bmatrix}$$

$$\times\ |\langle I\|T^{(1)}(n)\|I\rangle|^2 \sum_{J'} \frac{\langle J\|T^{(1)}(e)\|J'\rangle\langle J'\|T^{(1)}(e)\|J\rangle}{E_J - J'}$$

where

$$T^{(1)}(n) = \frac{\mu_I \vec{I}}{I} \quad \text{and} \quad T^{(1)}(e) = -\frac{H_e \vec{J}}{J} \ .$$

C. Nuclear Structure

There is a wealth of data about the ground and low excited states of nuclei. In particular, ABMR methods have been used to measure

spins I and electromagnetic moments (μ_I, Q_I, etc.) with considerable precision.

From the body of data it is found, for example, that nuclear ground state spins satisfy the following empirical rules:

(a) All nuclei with Z even and (A-Z) even have zero spin.

(b) Nuclei with A odd have half-integral spins.

(c) Nuclei with Z odd and (A-Z) odd have integral spins.

(d) Nuclei that contain the so-called magic number of protons (and/or neutrons) appear very stable. These magic numbers are 2, 8, 20, 28, 50, 82, and 126.

Various nuclear models have been constructed to explain the above observations and to calculate some other related nuclear properties. Two of the most successful are the shell[17] and collective[18] models. The shell model has been successful in explaining a great deal of the empirical data and it seems particularly applicable to the germanium nuclei. We therefore concentrated primarily on those aspects of the shell model relevant to the subject of nuclear spins and moments.

In this model, nucleons are assumed to move independently of one another in some spherically symmetric potential well. This potential is intermediate in shape between a harmonic oscillator potential and a rectangular well. The transition from the former to the latter proceeds as A increases. In addition, there is also a strong negative spin-orbit interaction of the form $[-f(r)\vec{\sigma}\cdot\vec{L}]$ where $\vec{\sigma}$ and $\vec{L}$ are the Pauli spin and orbital angular momentum operators, respectively, for a single nucleon.

The states are labelled by a set of quantum numbers, $|n\ell jm\rangle$, where n = total quantum numbers, ℓ = orbital quantum number, the total angu-

lar quantum number is $j = \ell \pm 1/2$, and m takes the values $+j, j-1, \cdots, 0, \cdots, -j$.

In a given nucleus these $|n\ell jm\rangle$ levels are filled up by neutrons and protons according to the Pauli Exclusion Principle. The energy levels resulting from such a model are shown in Fig. 2. With suitable adjustment of the shape of the well and strength of the spin-orbit interaction, this model accounts for all the magic numbers at closed shells of 2, 8, 20, 28, 50, 82, and 126 nucleons. Nuclei which contain these numbers of neutrons or protons are unusually stable.

The nucleons couple their angular momentum by j-j coupling to a resultant angular momentum or spin I. Closed shells of nucleons have, therefore, zero spin. It is further assumed that an even number of netrons or protons in a given level couple to zero spin, while an odd number couple to the spin of that level.

Therefore, according to this scheme,

(a) All even-even nuclei have zero spin.

(b) Nuclei with odd numbers of protons and even numbers of neutrons have the spin of the last odd proton, or vice versa.

However, for odd-odd nuclei, the spins cannot be predicted by the above scheme, as the separate angular momenta of the odd neutron and odd proton can be coupled to form several different resultant spins.

Nordheim[19] has formulated empirical rules for coupling j_p of the last proton to the j_n of the last neutron:

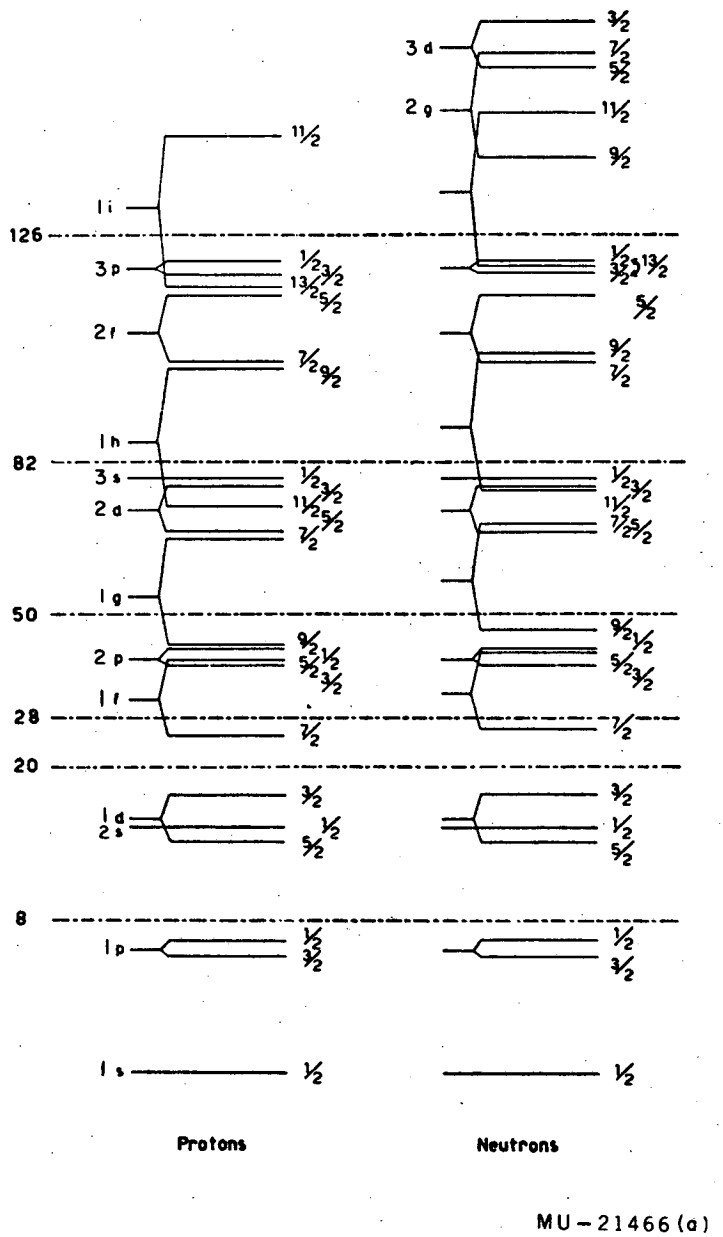

Fig. 2. Shell model single particle energy levels (spin-orbit and Coulomb energy terms included).

$$\left.\begin{array}{ll} \text{(a)} & \text{If } j_p = \ell_p \pm 1/2 \text{ and } j_n = \ell_n \pm 1/2, \text{ then } I > |j_p - j_n| \quad . \\ \text{(b)} & \text{If } j_p = \ell_p \pm 1/2 \text{ and } j_n = \ell_n \mp 1/2, \text{ then } I = |j_p - j_n| \quad . \end{array}\right\} \tag{55}$$

Brennan and Bernstein[20] have more recently modified the Nordheim rules to account for many more of the observed spins of odd-odd nuclei.

For configurations in which the odd protons and odd neutrons are both particles or holes:

$$\left.\begin{array}{ll} \text{(a)} & I = |j_p \pm j_n| \text{ if } j_p = \ell_p \pm 1/2 \text{ and } j_n = \ell_n \pm 1/2 \quad . \\ \text{(b)} & I = |j_p - j_n| \text{ if } j_p = \ell_p \pm 1/2 \text{ and } j_n = \ell_n \mp 1/2 \quad . \end{array}\right\} \tag{56}$$

If j_p or $j_n = 1/2$, then $I = |j_p - j_n|$. For configurations that are mixtures of particles and holes:

$$I = |j_p + j_n - 1| \quad .$$

We next examine the values of the electromagnetic moments of odd A nuclei as predicted by the shell model. It consists in evaluating the following quantities:

$$\left.\begin{array}{l} \mu_I = \langle Im|\vec{\mu}|Im\rangle_{m=I} \\ Q_I = \langle Im|\underset{\sim}{Q}|Im\rangle_{m=I} \\ \text{where} \\ \vec{\mu} = \dfrac{e\hbar}{2mc}\displaystyle\sum_{k=1}^{A} g_\ell^{(k)}\vec{\ell}^{(k)} + \dfrac{e\hbar}{2mc}\displaystyle\sum_{k=1}^{A} g_s^{(k)}\vec{s}^{(k)} \\ \underset{\sim}{Q} = \displaystyle\sum_{k=1}^{A} e^{(k)}\,(3\vec{z}_k^{\,2} - \vec{r}_k^{\,2}) \quad . \end{array}\right\} \tag{57}$$

This gives

$$\mu_I = \langle \mu_z \rangle_{m=I} = \frac{\mu_o I}{I(I+1)\hbar}\langle g_\ell\, \vec{L}\cdot\vec{I} + g_s\, \vec{S}\cdot\vec{I}\rangle_{m=I} \tag{58}$$

where we have used the well-known relation

$$\langle A_z \rangle_m = \frac{m}{I(I+1)\hbar}\langle \vec{A}\cdot\vec{I}\rangle_m$$

for the expectation value of the z-component of a vector operator A where I is the total angular momentum operator. Equation (58) can be written in the following form:

$$\mu_I = \frac{\mu_o I}{2I(I+1)\hbar} \langle g_\ell(I^2+L^2-S^2) + g_s(I^2+S^2-L^2)\rangle_{m=I}$$

$$g_I I = \frac{I}{2}\,[g_\ell+g_s) + (g_\ell-g_s)\,\frac{\ell(\ell+1) - 3/4}{I(I+1)}] \qquad (59)$$

where $I = \ell \pm 1/2$, and g_ℓ and g_s are the orbital and spin g-factors for the odd nucleon, taking the values

$$g_\ell = 1 \text{ for protons}$$
$$ = 0 \text{ for neutrons}$$

$$g_s = 5.587 \text{ for protons}$$
$$ = -3.826 \text{ for neutrons} \quad .$$

g is the nuclear g-factor.

Equation (59) may be written in the following form:

odd particle	$I = \ell \pm \frac{1}{2}$	$I = \ell - \frac{1}{2}$
proton	$\mu = (I+\frac{1}{2}+\frac{1}{2}g_s)\mu_N$	$\mu = [I+\frac{I}{I+1}(\frac{1}{2} - \frac{1}{2}g_s)]\mu_N$
neutron	$\mu = \frac{1}{2}g_s\mu_N$	$\mu = -\frac{I}{I+1}\cdot\frac{1}{2}g_s\mu_N$. (60)

where μ_N is the nuclear magneton. These are known as the Schmidt moments.[21] The fact that most observed moments differ from the Schmidt values has been explained in a number of ways. One approach is to use quenched g-factors rather than free-nucleon g-factors. The latter are considered to be modified in the nucleus by the presence of meson-exchange currents. It is customary to modify g_s to make Eq. (59) fit observed moments. Similarly, the electric-quadrupole moment is given by[22]

$$Q = Q_j = -\left(\frac{2j-1}{2j+1}\right)\langle r^2\rangle \quad \text{for odd proton}$$

$$Q = Q_j \approx \frac{Z}{(A-1)^2} Q_j \quad \text{for odd neutron.} \tag{61}$$

By $\langle r^2 \rangle$ is meant the average of r^2 for the nucleon orbit, and this is usually replaced by $\frac{3}{5} R_o^2$ where R_o = nuclear radius. For odd-odd nuclei, Ref. 22 gives the magnetic moment if j-j coupling is used:

$$\mu = \frac{1}{2}(g_n+g_p) + (g_p-g_n) \frac{j_p(j_p+1) - j_n(j_n-1)}{2(I+1)} \quad . \tag{62}$$

We also note that recent quasi-particle theories[23] have been used to calculate nuclear moments which agree more with observed values than the Schmidt values do.

III. ATOMIC-BEAM MAGNETIC-RESONANCE METHOD

A. General Description of Apparatus

Figure 3 is a schematic diagram of a typical atomic-beam "flop-in" machine. It consists of an oven O (serving as source of atoms), three magnetic field regions, and a detector. The magnets labelled by the letters A and B are inhomogeneous magnets, whose field gradients are oriented as shown in the figure. These fields are strong enough to decouple the electronic and nuclear angular momenta. The magnet labelled C produces a homogeneous field. A radiofrequency hairpin, situated in this region, causes transitions between magnetic sub-levels of the atom.

An atom with a non-zero electronic magnetic moment, which effuses out of oven O, is deflected while passing through the A-magnet region. In the C-magnet region, it may or may not undergo a resonant transition. Should it undergo one, the sign of its m_J changes. The B magnet is designed in a way that such an atom will experience a deflection in this region to counteract that produced by the A magnet. Thus the atom will be deflected onto the detector D. These trajectories can be explained as follows:

An atom with electronic magnet moment $g_J \mu_o \vec{J}$ and nuclear magnetic moment $g_I \mu_o \vec{I}$ in an external magnetic field $\vec{H}_o$ has energy

$$W_{mag} = -g_J \mu_o \vec{J} \cdot \vec{H}_o - g_I \mu_o \vec{I} \cdot \vec{H}_o \quad .$$

Usually the magnetic field is large enough to make the high field scheme discussed in Section II valid and hence the energy is

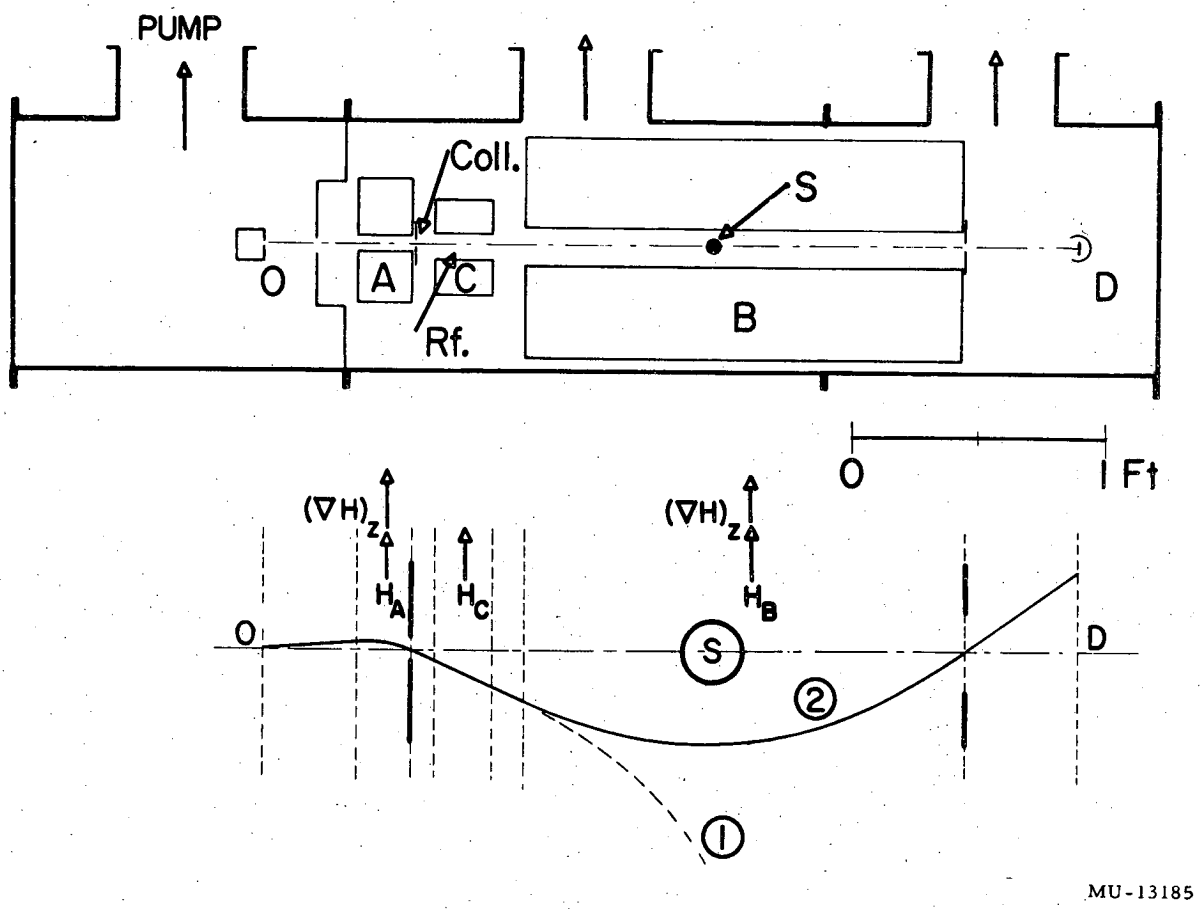

Fig. 3. Schematic of flop-in atomic beam machine. O, oven; S, stop wire; A,B, inhomogeneous magnets; C, homogeneous magnet; D, detector; 1, path of non-resonant atoms; 2, path of resonant atoms.

$$W_{mag} = -g_J \mu_o m_J H_o - g_I \mu_o m_I H_o \quad .$$

If $\vec{H}_o$ is non-uniform, the atom experiences a force proportional to the gradient of the field and to the effective magnetic moment:

$$\vec{F} = -\nabla \vec{W} = -\frac{\partial W}{\partial H_o} \nabla \vec{H}_o \equiv \mu_{eff.} \nabla \vec{H}_o$$

$$= (g_J \mu_o m_J + g_I \mu_o m_I) \frac{\partial \vec{H}}{\partial z} \quad .$$

Since

$$g_I / g_J \approx \frac{m_e}{m_p} \approx \frac{1}{2000} \quad ,$$

$$\vec{F} \approx g_J \mu_o m_J \frac{\partial \vec{H}}{\partial z} \quad .$$

It is clear that the deflection depends on the value of m_J. Also, in order that the atom be refocused by the B-magnet when the sign of the field gradients in both A and B region is the same, it is necessary that

$$m_J (A_{mag}) = -m_J (B_{mag}) \quad .$$

Two cases occur in which atoms may still strike the detector without undergoing a transition in the C-magnet region: (a) atoms with $m_J = 0$, which experience little or no deflection and hence reach the detector regardless of whether or not a transition takes place in the C region, and (b) very fast atoms for which the force acts only a short time. Both types would contribute a large background. Hence an obstacle S is placed in the B-magnet region to block these atoms while allowing atoms following a flop-in path to reach the detector.

The types of transitions that can be induced by the weak radio-frequency field $\vec{H}_{rf}$ in the C-magnet region are limited by both machine selection rules and magnetic dipole selection rules.

In the low-field region, F and m_F are good quantum numbers. Hence, permissible transitions are

$$\Delta M_F = 0 \quad \Delta F = \pm 1$$

$$\Delta m_F = 1 \quad \Delta F = 0, \pm 1 \quad .$$

In the high-field region, I and J are decoupled and the selection rules are

$$\Delta m_J = 0, \quad \Delta m_I = \pm 1$$

$$\Delta m_J = \pm 1, \; \Delta m_I = 0$$

In addition to these, there is always the machine selection rule which requires that for an atom to be refocused,

$$m_J \; (A) = - \; m_J \; (B) \quad .$$

The detectors in the atomic-beam machine are of two kinds. One is a hot tungsten wire located at the center of the flop-in path. Refocused atoms impinge on it and are ionized. The ion current is collected and measured by an electrometer. This works for easily-ionized atoms like the alkali atoms, which in our machine are used to calibrate the magnetic field.

The other is the radioactive detector, which consists of two sulfur-coated brass buttons. One is placed on the machine axis to collect the beam of flopped-in atoms; the other collects the flopped-out beam. Both are exposed simultaneously for five minutes with a given $\vec{H}_{rf}$ in the C-field region. The buttons are then sent to the counting room three floors up and about 500 feet away from the

experimental room. The resonance signal is taken as the ratio of the center activity to the side activity.

Our experiments were performed on the Berkeley atomic-beam machine II. A complete description of the apparatus, save for one or two modifications and repairs, has been given by Dabbousi.[24]

The modifications are:

(a) The oven loader: a new oven loader was designed. Its general shape and dimensions were the same as the old ones. The cooling system was considerably modified, which completely eliminated the perrenial problem of water leakage. This was achieved by connecting the external flange directly through the water cooling pipes to the copper head holding the oven. The design also facilitates leak detection. Figure 4 is a picture of the new design.

(b) The C-magnet: this has also been considerably redesigned by Dr. Schmelling. The C-field range has now been extended from a previous upper limit of about 400 gauss to the new limit of 2000 gauss. The design is such that the magnet field has a linear relation with the magnet current and does not saturate, as the old magnet did. Figure 5 shows the new C-magnet design.

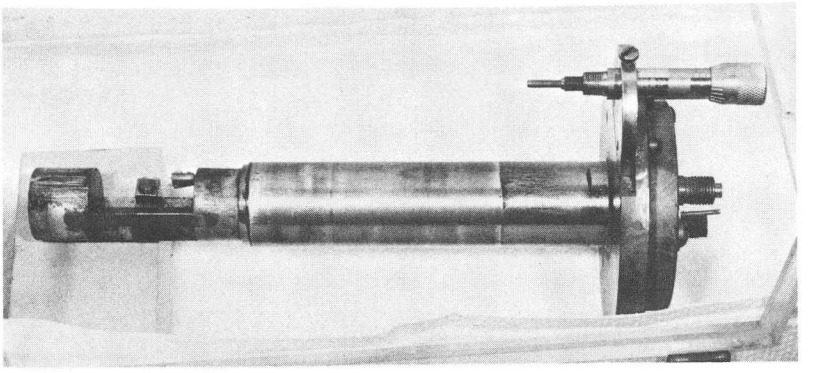

XBB 699-6129

View 1. Oven loader with a tantalum oven in place.

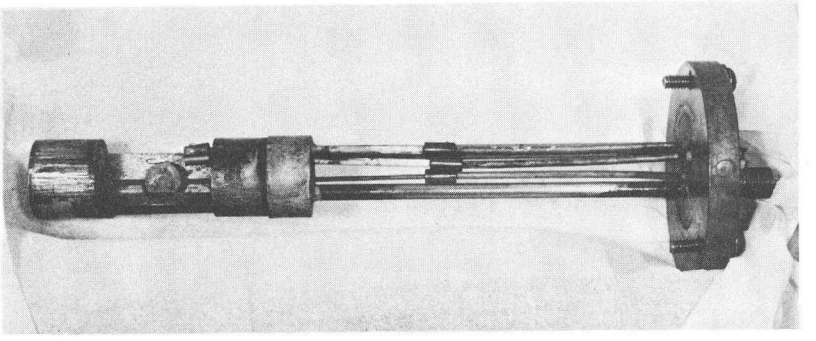

XBB 699-6130

View 2. Oven loader showing the new design of the water cooling system.

Fig. 4. The new oven loader.

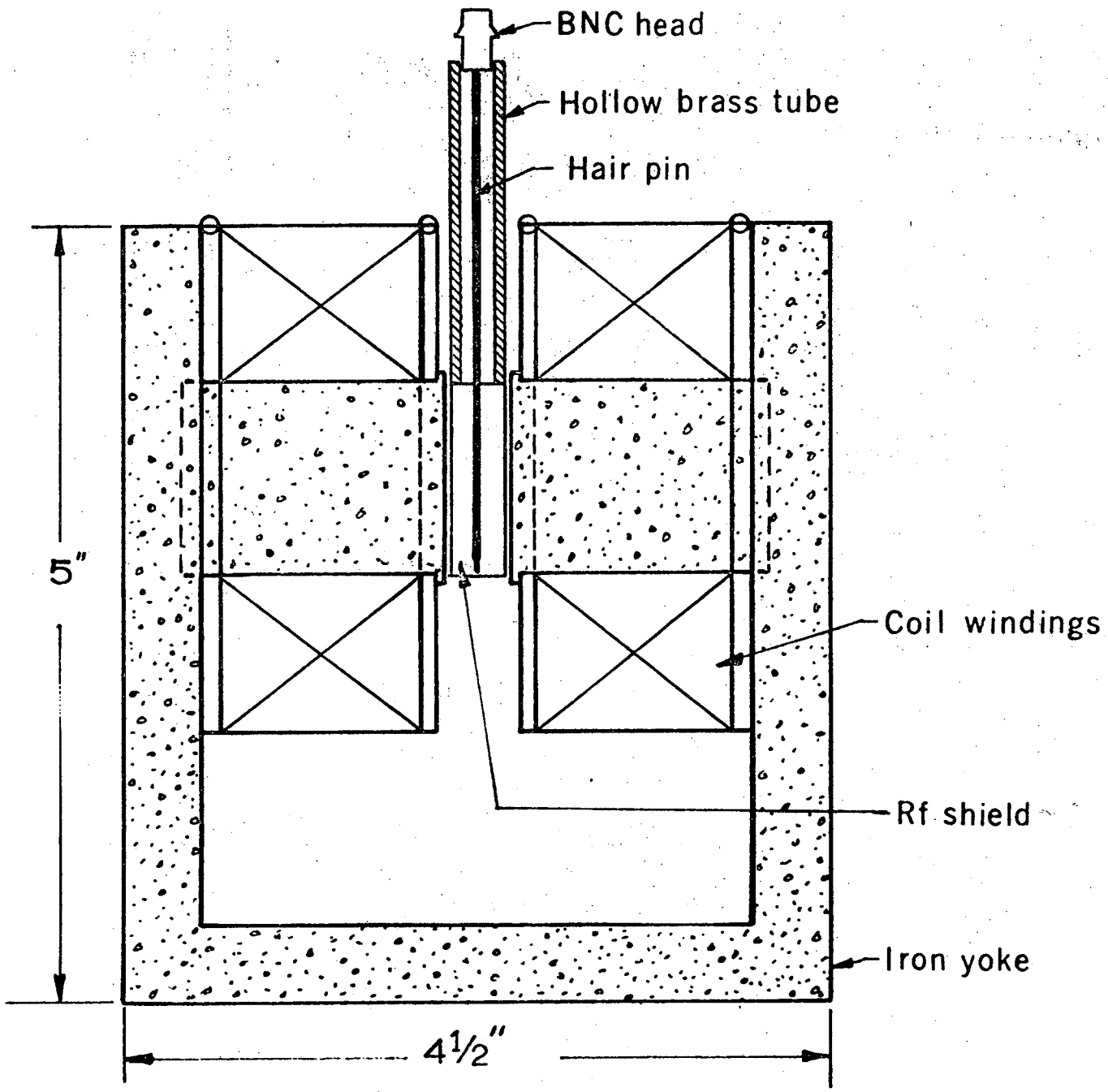

Fig. 5. Schematic sketch of the new C-magnet design.

IV. EXPERIMENT

A. Ge Isotopes

The electronic ground state configuration of the germanium atom is $4s^2\ 4p^2$. In order of increasing excitation energy, the states arising from this configuration[25] are $^3P_0$ (the electronic ground state), $^3P_1$, $^3P_2$, $^1D_2$, and $^1S_0$. At the temperature of the atomic beam (∿1400°C) the Boltzmann factors of the $^3P_1$ and $^3P_2$ states are large enough to make transitions between hyperfine levels in these states observable (Table I).

Both states have an integral electronic angular momentum J. This means there will be an $m_J = 0$ state present. The machine selection rule requires that $m_J(A) = -m_J(B)$. This will require an atom to go from the state $m_J(A) = \pm 1$ to state $m_J(B) = \mp 1$ in order to follow the flop-in path. Two quanta are needed to achieve this. The frequency put in is half that required for transition from state A to state B. With sufficient rf power 2 quanta may be absorbed to cause transition from A to B with an intermediate virtual level; this is the double-quantum transition. It is always encountered in atomic-beam experiments using atoms with integral J values. The two-frequency method is even simpler, and will be discussed later in Section IV.B.4.

B. ^{75}Ge

1. Production and Detection

The radioactive ^{75}Ge isotope has a half-life of 82 minutes. It is easily produced in a nuclear reactor by the reaction

$$^{74}Ge\ (n, \gamma)\ ^{75}Ge$$

on 36.74% abundant naturally occurring ^{74}Ge.

Table I. Ge beam properties.

State	Energy (cm^{-1})	Boltzmann Factor $e^{-E/kt}$	% of Beam	g_J
$^3P_0$	0.00	1.00	51	
$^3P_1$	557.10	0.64	32.6	-1.50111(7)
$^3P_2$	1409.90	0.32	16.3	-1.49458(9)
$^1D_2$	7125.26	0.003	0.1	
$^1S_0$	16367.14	$\approx 10^{-4}$	~ 0.0	

The cross-section for this reaction is about 0.3 barns. About 100 mg of a natural Ge, previously melted into spheres, was encapsulated in quartz and irradiated in the Berkeley TRIGA MARK III reactor, which has a flux of 10^{13} neutrons/cm^2/sec. A bombardment of 3 hours produced enough activity, usually about 0.1 curie, to last through three half-lives of running time. We also found that over 95% of the activity produced belonged to ^{75}Ge. The remaining 5% belonged to ^{77}Ge and ^{71}Ge. Furthermore, no chemistry was necessary, as Ge metal was used. As only about 30 minutes elapsed from the time the sample was taken out of the reactor until it was loaded into the oven and transferred into the machine, it decayed less than one half-life between the end of the bombardment and the start of the experiment.

2. Beam Formation

Our ovens are made of tantalum lined with a carbon crucible and lid to avoid any reaction between the germanium and tantalum; Figure 6 is an illustration of the oven and its component parts.

Electron-bombardment power, typically around 150 to 200 watts, heated the oven to operating temperatures of between 1300° and 1500°. At these temperatures enough atoms are excited to both $^3P_1$ and $^3P_2$ states to make atomic-beam research possible. At the start of each run, normalization (side button) signals of about 1500 counts/min. were produced, with corresponding resonance signals of from 50 to 300 counts/minute.

To detect ^{75}Ge, its β-ray emission during decay was utilized. Thin-window Geiger counters counted the emitted β-rays. Each counter is surrounded by a guard counter to reduce the background from

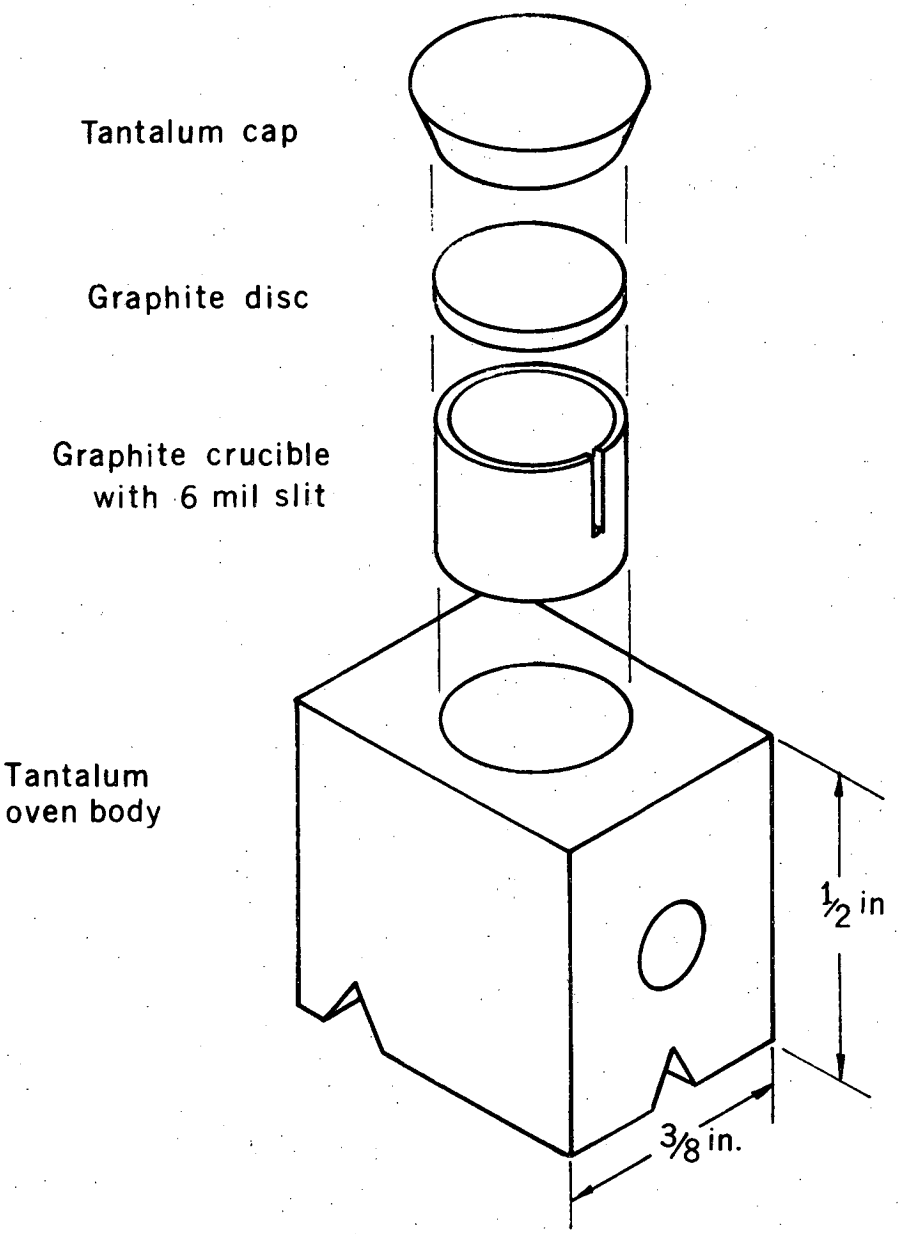

XBL 699 4915

Fig. 6. Exploded view of carbon-lined tantalum oven used to produce beams of germanium atoms.

extraneous radiation; typical background counts range from 4 to 8 counts/minute. For better statistics, the spin or central buttons were cycled through three or four such counters for 5 minutes each, while the normalization button was counted in one counter. Figure 7 shows the setup of a β-counter.

3. Spin Measurement

We achieved the initial spin measurement for ^{75}Ge by observing $\Delta F = 0$ transitions at very low fields. The frequency of such transitions is given by

$$\nu_o = g_F \frac{\mu_o}{h} H_o \quad . \tag{63}$$

In our case, as Ge has integral J values, we had to induce a double-quantum transition, explained at the beginning of this section. The magnetic field H_o was set at a value that separated the frequencies predicted for each value of I by at least one line-width. Buttons were then exposed at the frequencies predicted by Eq. (63).

Figure 8 shows the results of such a search at approximately 1 G. Large signals were obtained for I = 1/2 for the J = 1 state. Further, to establish the spin, a sweep was taken and resonances were obtained at the predicted values for spin I = 1/2 in the $^3P_1$ and $^3P_2$ states.

We further decayed the I = 1/2 signal for about 30 hrs. and a half-life of 82 minutes was obtained. This confirmed that the spin I = 1/2 belonged to ^{75}Ge as opposed to the other radio-isotopes of Ge. Figure 9 shows the decay curve.

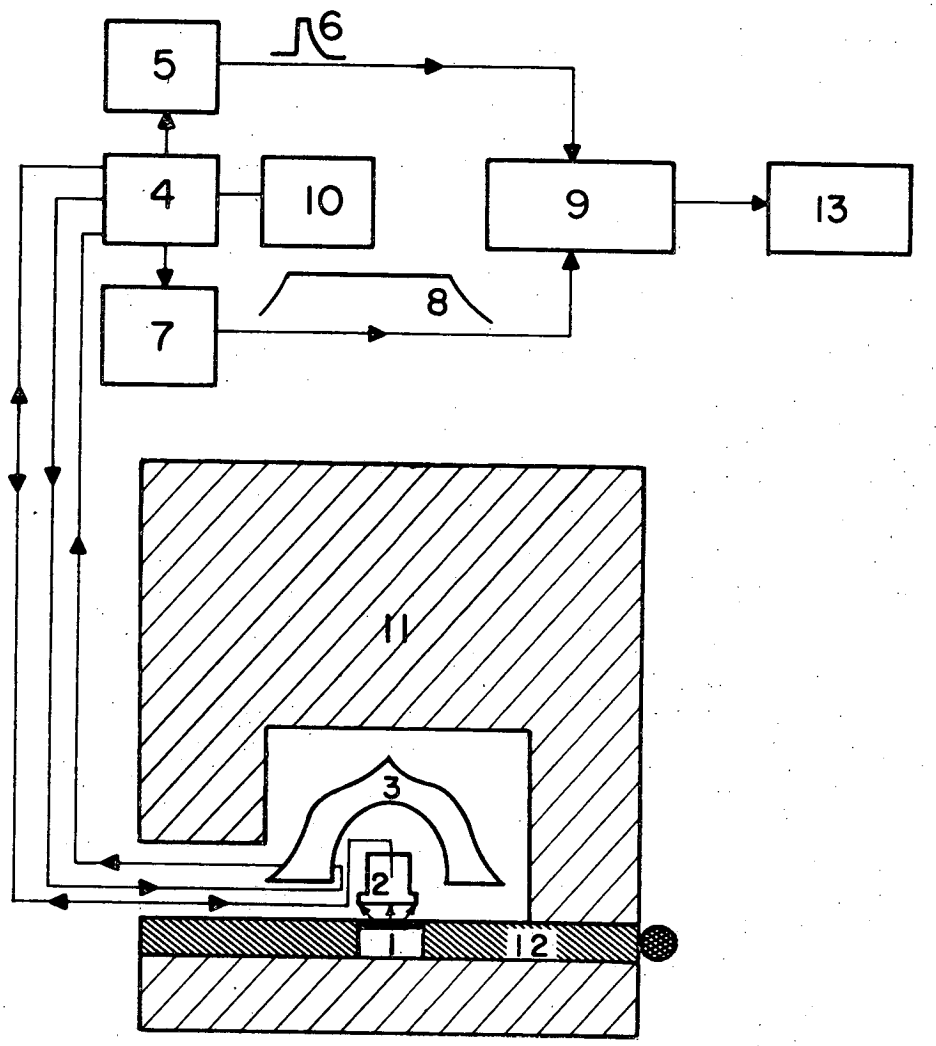

XBL674-2785

Fig. 7. Schematic of the beta-counter system. 1, radioactive button; 2, β-counter; 3, guard counter; 4, high-voltage divider and decoupler; 5, β-signal amplifier; 6, amplified β-signal (2 μsec wide); 7, guard signal amplifier; 8, amplified guard signal (30 μsec wide); 9, single-channel analyzer; 10, high-voltage supply; 11, lead pig; 12, brass drawer to hold button; 13, scaler.

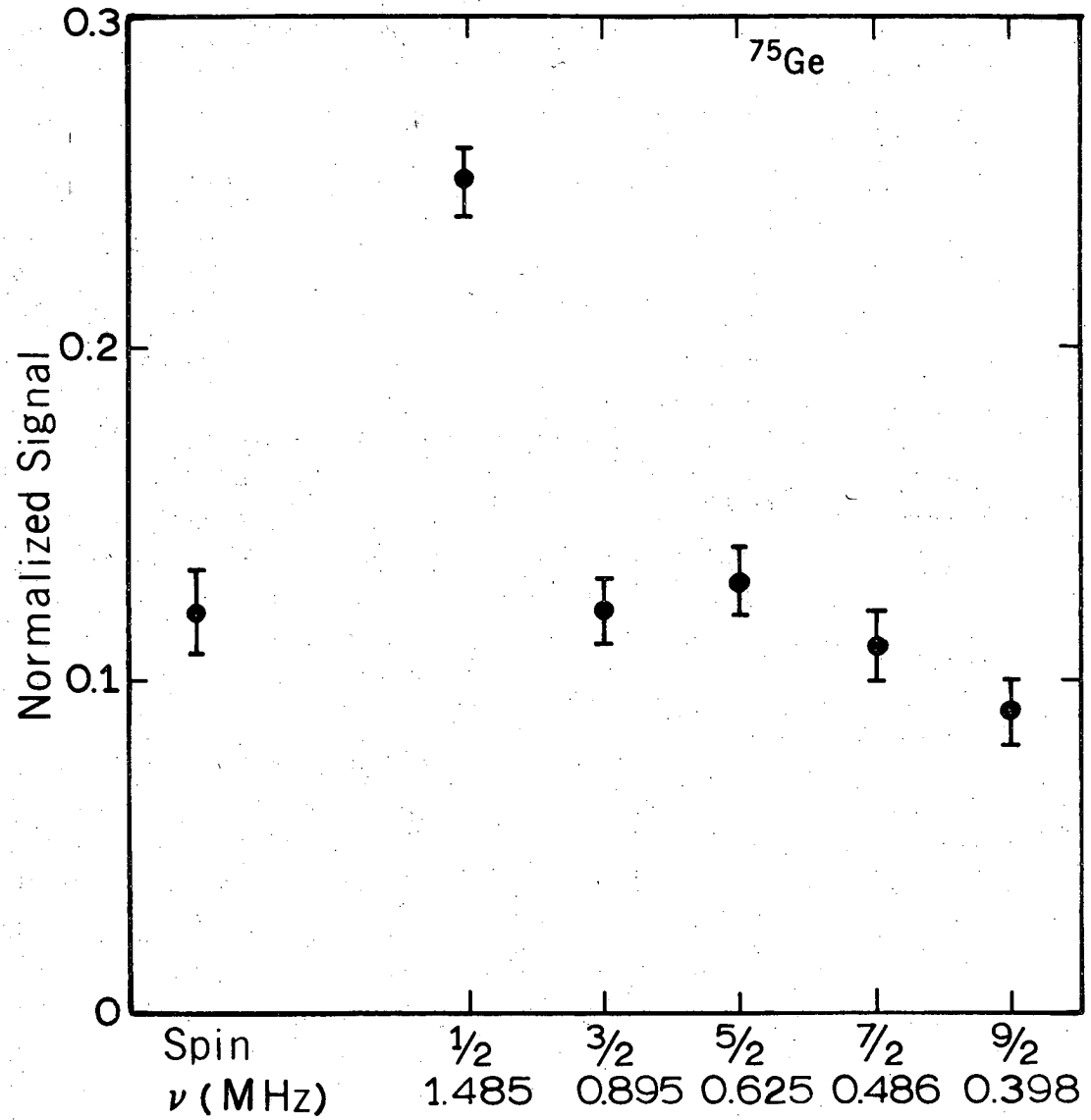

XBL 699 4900

Fig. 8. ^{75}Ge spin search at ∿1.05 gauss.

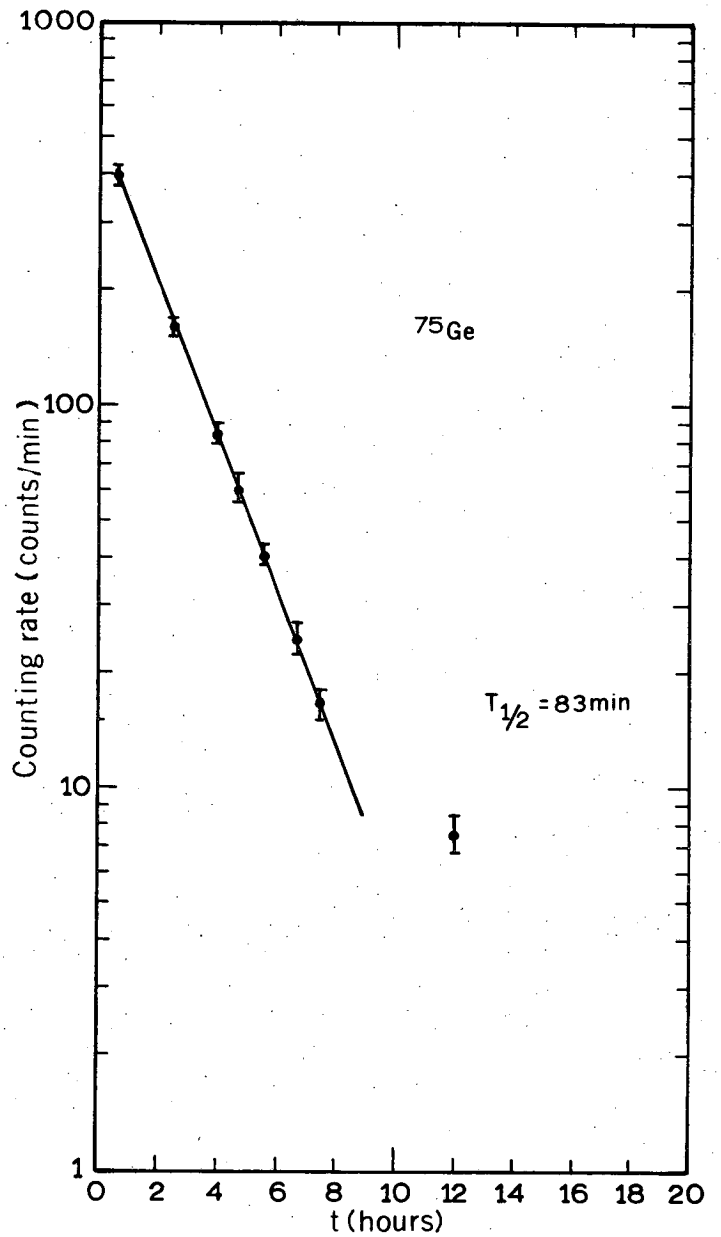

XBL 699 4901

Fig. 9. Decay of activity on I=1/2 button from ^{75}Ge.

4. Hyperfine Structure Measurement

A schematic diagram of the hfs diagram for ^{75}Ge is shown in Figure 10. All the transitions observed are labelled, i.e., α ($\Delta F = 0$, $\Delta m_F = 2$), β ($\Delta F = 1$, $\Delta m_F = 1$), and γ,δ ($\Delta F = 0$, $\Delta m_F = 1$).

The general procedure, as with other atomic-beam experiments, is to follow one of the resonances up to higher fields starting from the low-field Zeeman region. In the case of ^{75}Ge, the α-transition used in measuring the spin I was predictably followed up in magnetic field to about 20 gauss. This was a double-quantum transition. It was observable as long as two single-component transitions (γ, δ) differed by less than a few line-widths. At about 20 gauss the signal-to-background ratios had dropped considerably. In fact it was poorer than 0.5, whereas it was as high as 3 at 1 gauss.

Usually an increase in magnetic field introduces a small deviation from the linearity expressed by Eq. (63). This term, in general, is quadratic, and is due to the incipient decoupling of I and J by the external field. To second order in the field, the shifted frequency is then given by

$$\nu = \nu_o + \frac{2J\ \nu_o^2}{\Delta\nu}$$

where ν_o is the linear Zeeman frequency. The shift $(2J\ \nu_o^2)/\Delta\nu$ gives a rough estimate of $\Delta\nu$. This shift was increased by increasing the field until $\Delta\nu$ was determined to a reasonable accuracy. At this point all the information obtained from this transition still gave a large uncertainty in a.

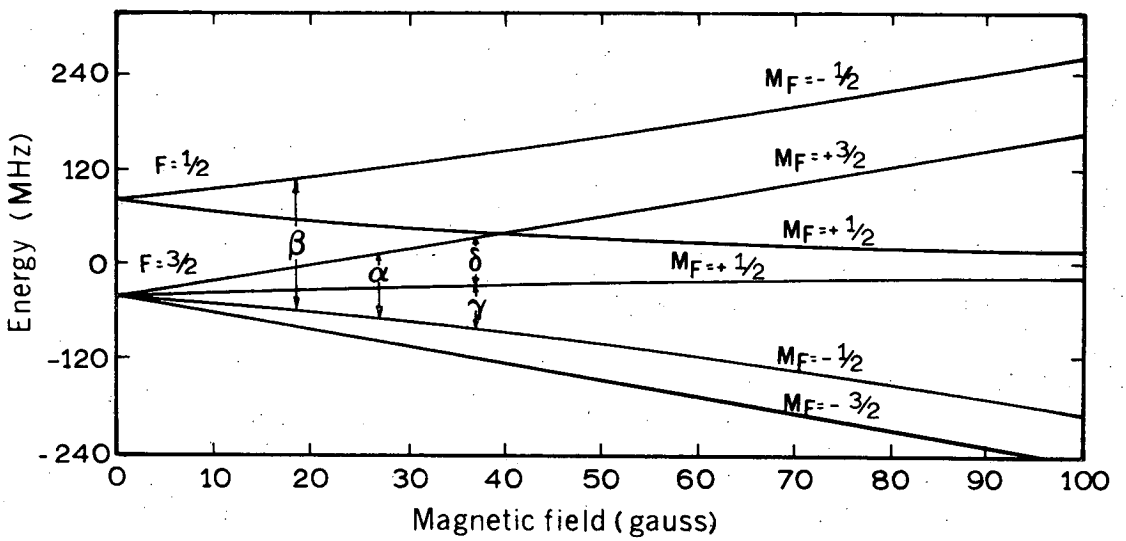

XBL 699 4902

Fig. 10. Energy level diagram for the $^3P_1$ hfs levels of 83-min ^{75}Ge with a<0.

At 20 gauss, the uncertainty in $\Delta\nu$ was still larger than 3 MHz. Another technique was tried. Instead of the single frequency for the double-quantum transition, two single frequencies were simultaneously fed in to match the frequencies predicted for the single-quantum transitions γ and δ. A good description of this technique has been given by Prior.[26]

Consider the three-level system shown in Fig. 11. Transition A→C represents the double-quantum transition, while Transitions A→B and B→C are the two single-quantum transitions γ and δ. The implementation of the two-frequency technique requires two rf generators, amplifiers, frequency counters, and a device for mixing the two frequencies before transmission to the hairpins.

One generator was set to match the predicted frequency for one of the transitions, say γ(A→B), and the other was varied until a signal corresponding to the δ(B→C) transition was observed. Next, the latter frequency was fixed at the observed δ resonance point and the frequency for the γ transition was varied until a resonance was again observed. A further third sweep could be taken by keeping the γ frequency fixed again and rechecking the δ resonance frequency. This process continued until the peak resonance frequencies became virtually constant.

Figure 12 illustrates the typical rf circuit for this technique.

Figure 13 shows a resonance sweep for a double-quantum transition at about 12 gauss, while Fig. 14 shows the two single-quantum resonances observed by the two-frequency technique.

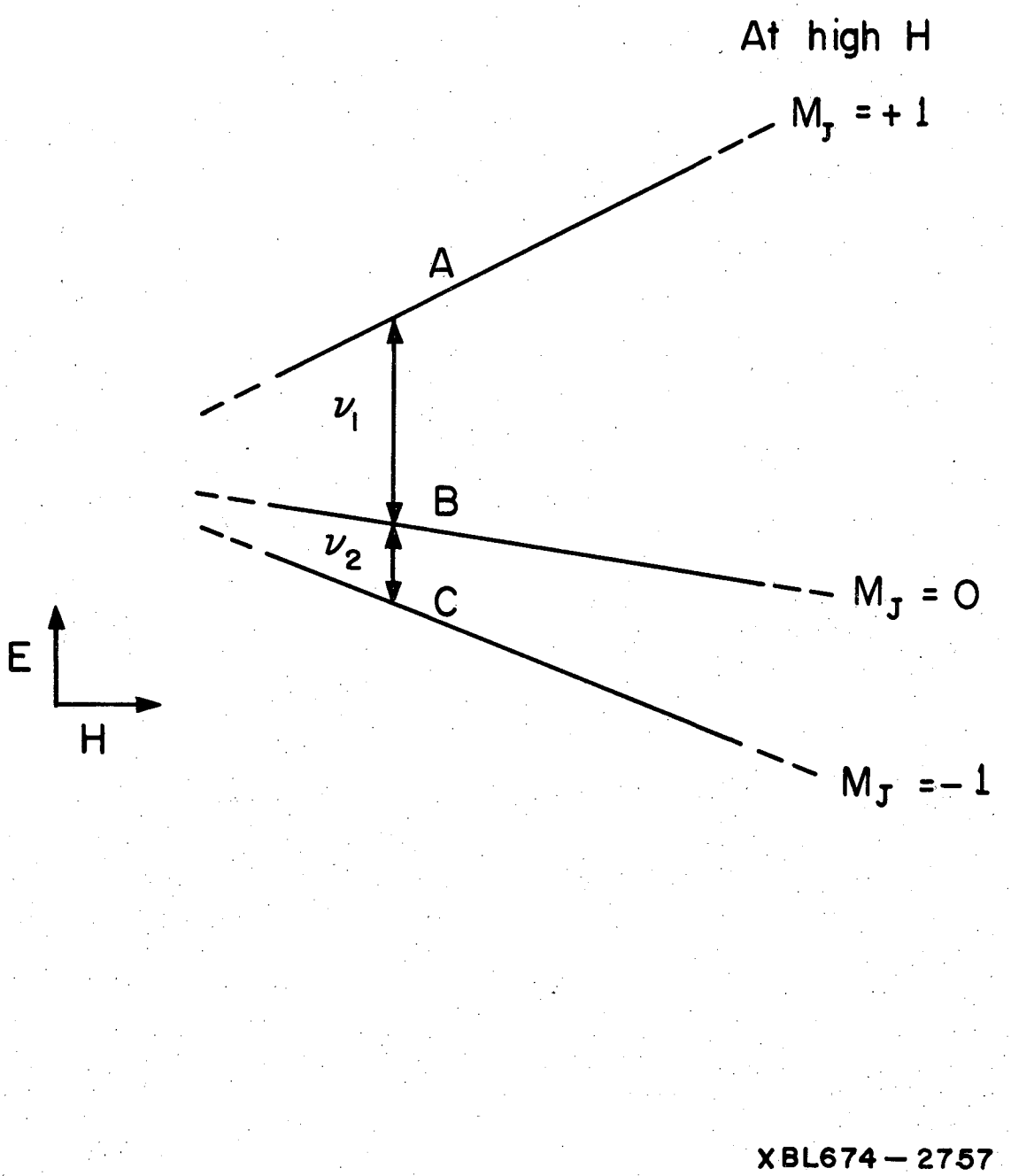

Fig. 11. Three-level system. ν_1, frequency for δ (A→B) transition; ν_2, frequency for γ (B→C) transition.

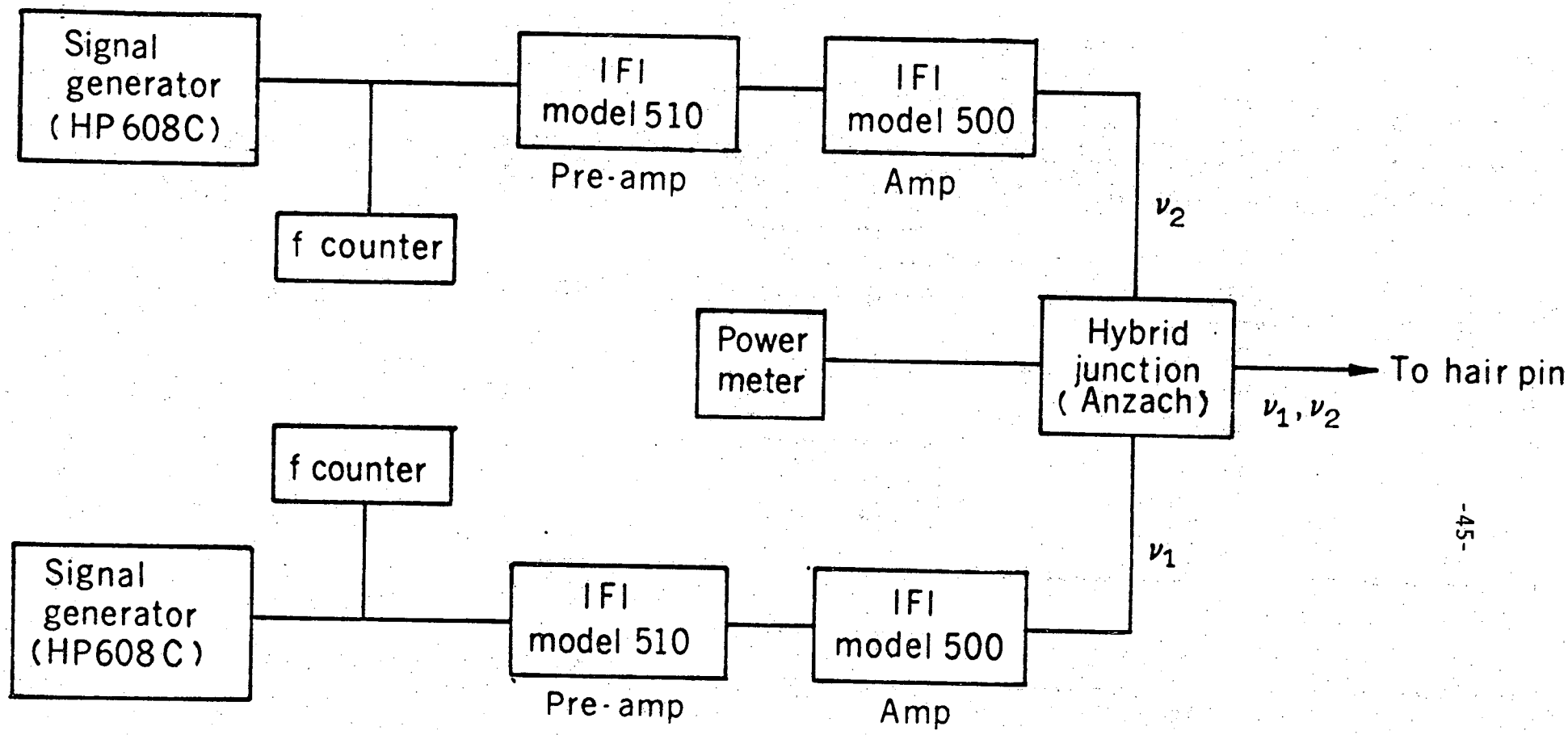

Fig. 12. The rf circuit for the two single-frequency method.

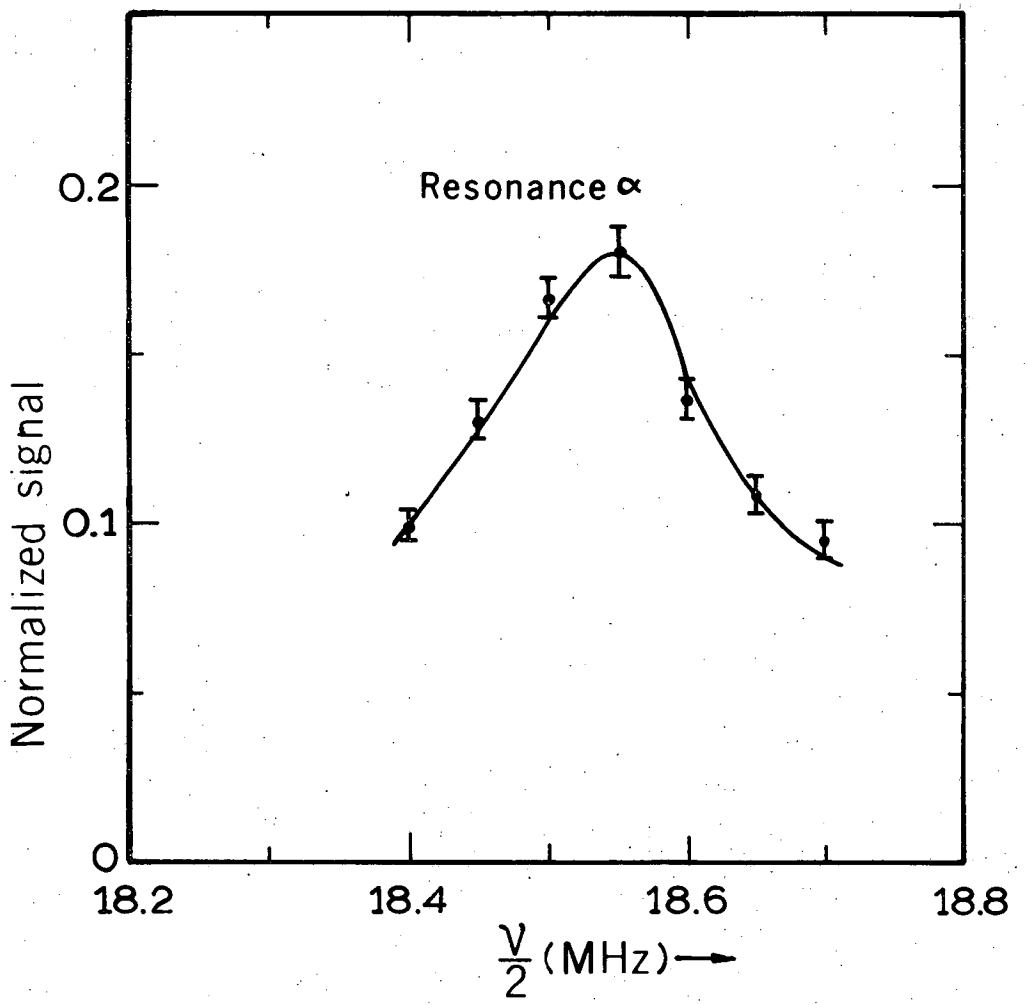

XBL 6994904

Fig. 13. ^{75}Ge double-quantum transition at ∿12.8 gauss. The levels connected are (F=1.5, M=0.5) and (F=1.5, M=1.5).

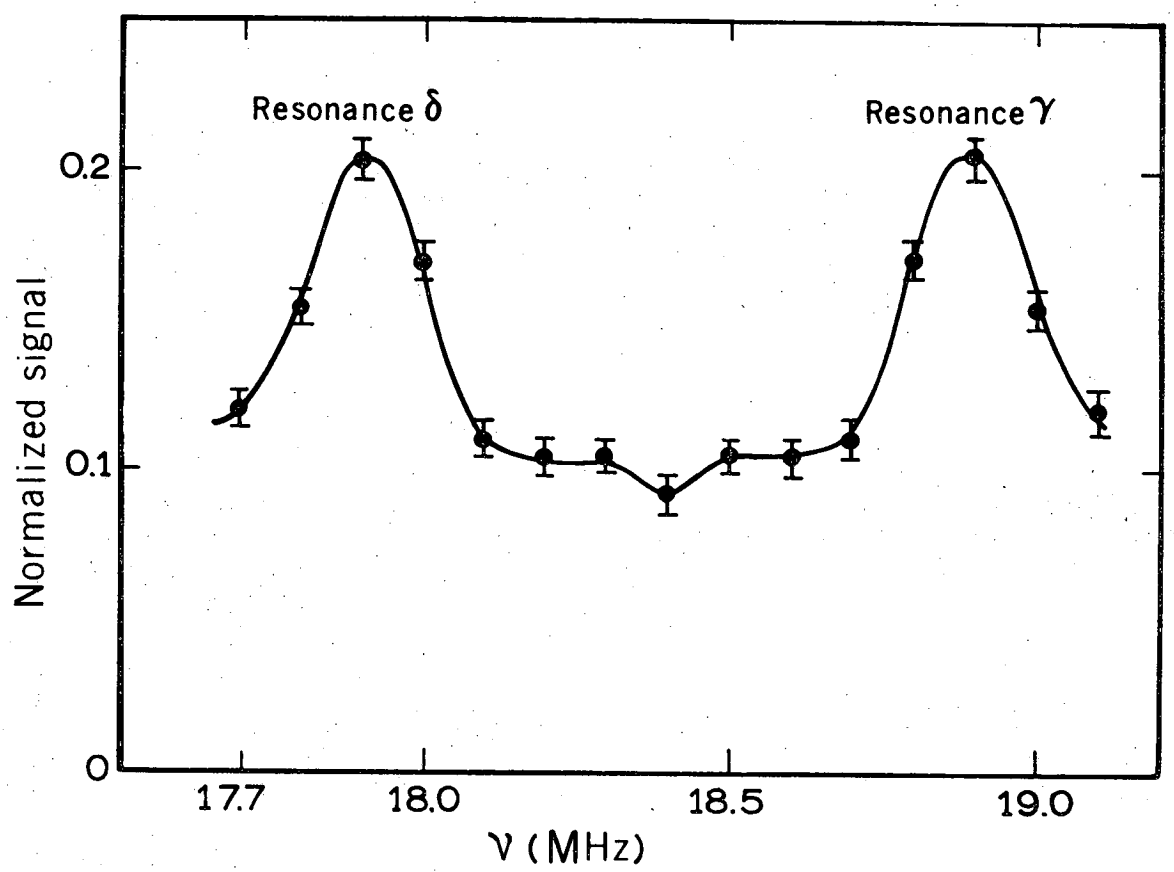

XBL 699 4905

Fig. 14. Two single-frequency resonances at ∿12.8 gauss. The levels connected in δ are (F=1.5, M=0.5) and (F=1.5, M=-0.5); those in γ are (F=1.5, M=-0.5) and F=1.5, M=-1.5).

This latter technique was used to follow the δ and γ transitions up to about 70 gauss, at which field the uncertainty in the hfs a was small enough to make it possible to look for the direct $\Delta F = 1$ transition (β-transition). Since for the $J = 1$ state

$$\Delta\nu = a(J + 1/2) = 3/2a \quad ,$$

a direct transition at very low fields accurately determines the hfs constant. Indeed, the best resonance signal for ^{75}Ge was obtained for the $\Delta F = 1$ transition at 1 gauss. The signal-to-background ratio was about 6.

Figures 15a and 15b show the transition. The size of the signal encouraged us further to pursue this β-transition to very high fields.

From the work of Goodman and Childs[16] on ^{73}Ge, the relative sign of hfs constant a and the nuclear magnetic dipole moment μ_I was known. To establish the absolute signs, we chose to follow the β-transition to very high fields ($\sim$150 gauss). At this field the difference in frequency for $\mu < 0$ and $\mu > 0$ was at least half a line-width. We did observe resonances at 100 G and 130 G to establish a positive sign for μ_I and, hence, a negative sign for hfs constant a. Figure 16 is the $\Delta F = 1$ resonance at 100 G. The arrows indicate the predicted points for $\mu < 0$ and $\mu > 0$. From Fig. 16, μ_I is shown to have a positive sign.

a. Hyperfine Structure for the $^3P_2$ State. At this point, one could predict with high accuracy the hfs constant $a(^3P_2)$ by comparing ^{75}Ge to ^{73}Ge and using the Fermi-Segrè relation. From Table I, we see that the percentage of the beam in the $^3P_1$ state is about twice that in the $^3P_2$ state. Also, there are 6 hyperfine levels in the $^3P_1$

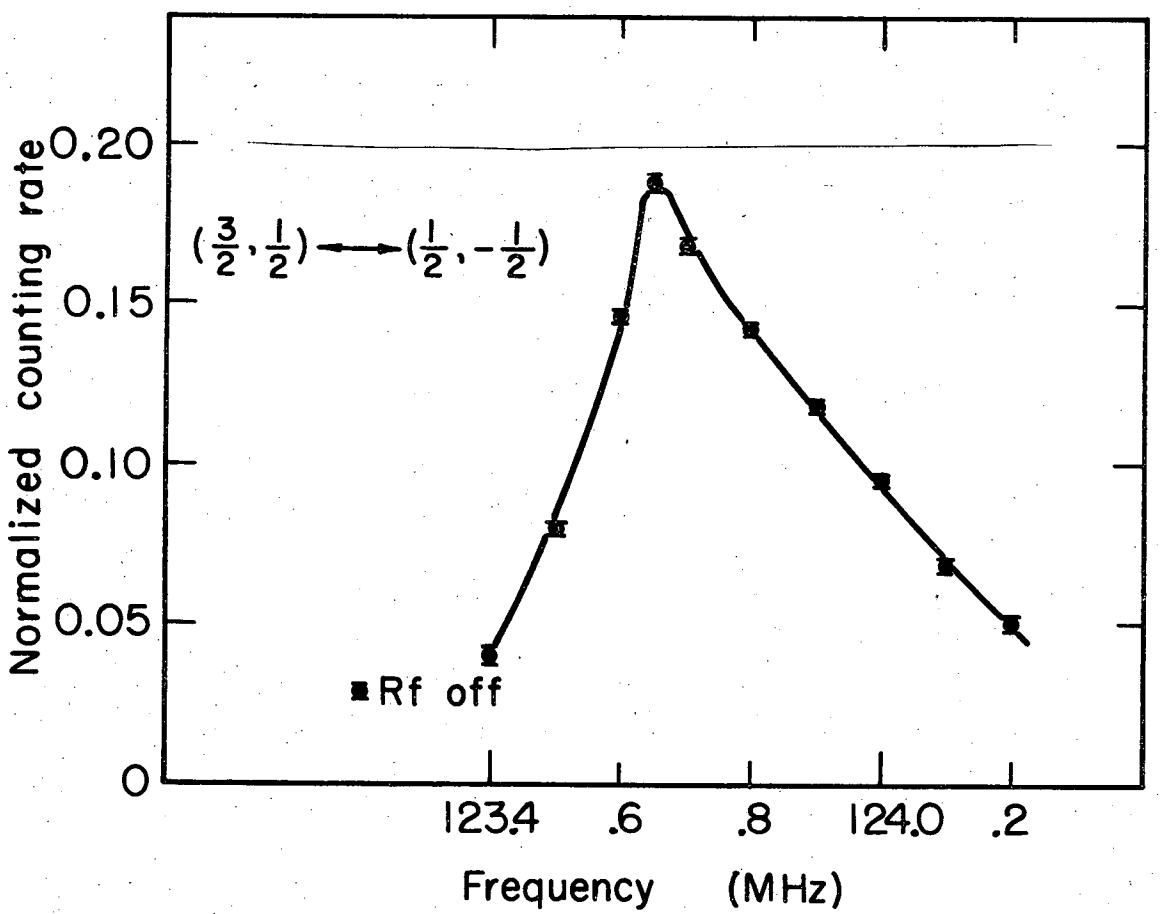

XBL6812-7393

Fig. 15a. $\Delta F=1$ transition in $^{75}Ge(^3P_1)$ at 1 gauss.

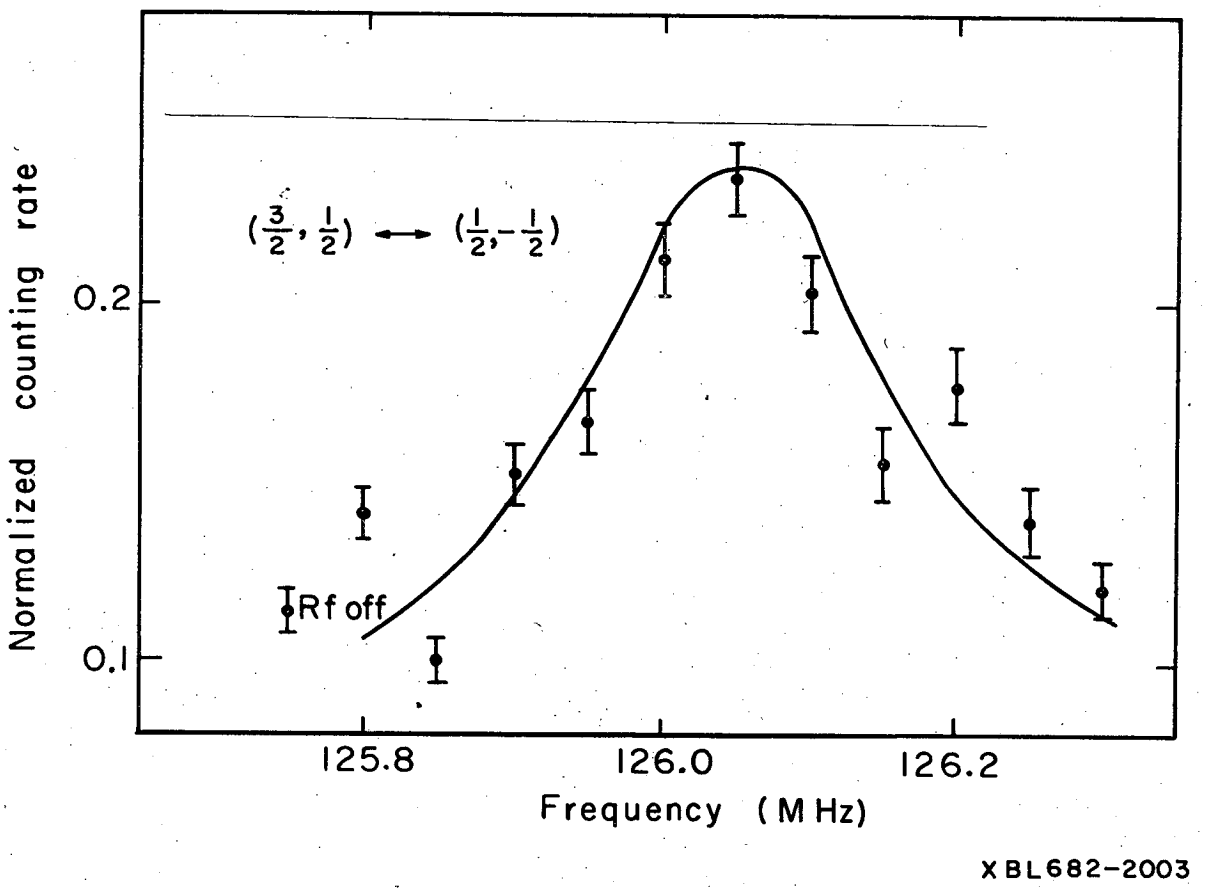

Fig. 15b. $\Delta F=1$ transition in $^{75}Ge(^3P_1)$ at 2.1 gauss.

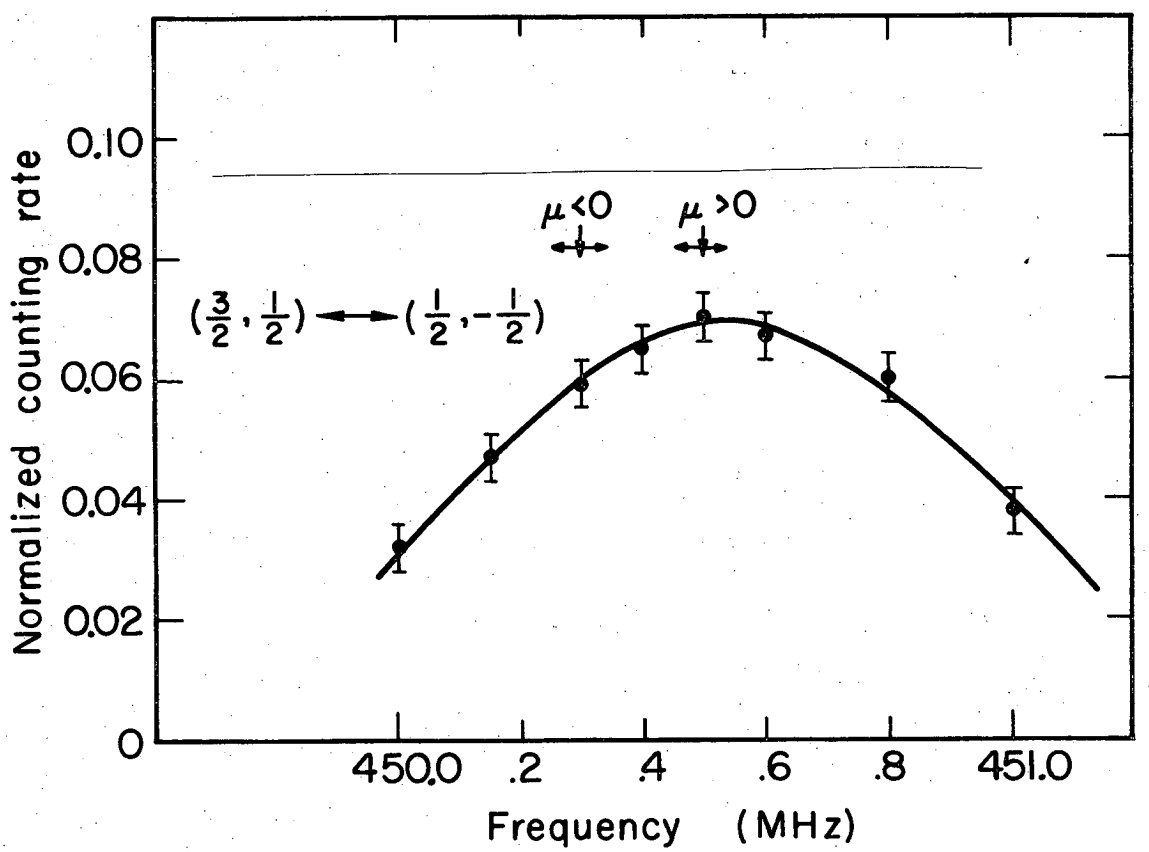

XBL6812-7390

Fig. 16. $\Delta F=1$ transition in $^{75}Ge(^3P_1)$ at 100 gauss. Testing sign of μ_I.

state compared to 10 for the $^3P_2$ state. Both facts led us to expect a much poorer signal for the $^3P_2$ direct transition than for the $^3P_1$ direct transition. In fact, it took several runs before we could obtain a good signal. This was after the activity of ^{75}Ge was increased beyond the level sufficient for good signals in the $^3P_1$ state.

Direct transitions were obtained at 1 to 5 gauss; Figure 17 shows one at 5 gauss.

This transition is labelled β in the schematic Breit-Rabi diagram in Fig. 18.

5. Results

For the $^3P_1$ state, a total of 23 resonances ($\Delta F = 0$ and ± 1), listed in Table II, were observed. A least squares fit[11] (by the computer routine HYPERFINE) of the calculated frequencies to the observed resonances yielded the results listed in Table III. Table IV lists the results for the $^3P_2$ state for which a total of 5($\Delta F = 0$ and ± 1) were observed.

The numbers in parentheses indicate the error in the least significant figure and represents two standard deviations for a. This gives a confidence level of above 90%. The magnetic moment was calculated using the Fermi-Segrè relation by comparing ^{75}Ge to ^{73}Ge. The nuclear moments[28] and hfs constants of the stable ^{73}Ge isotope have been measured[16] previously. The listed values are shown in Table V.

The error in μ_I for ^{75}Ge is taken to be 1% to allow for a possible hfs anomaly. The difference in χ^2 between the fits for

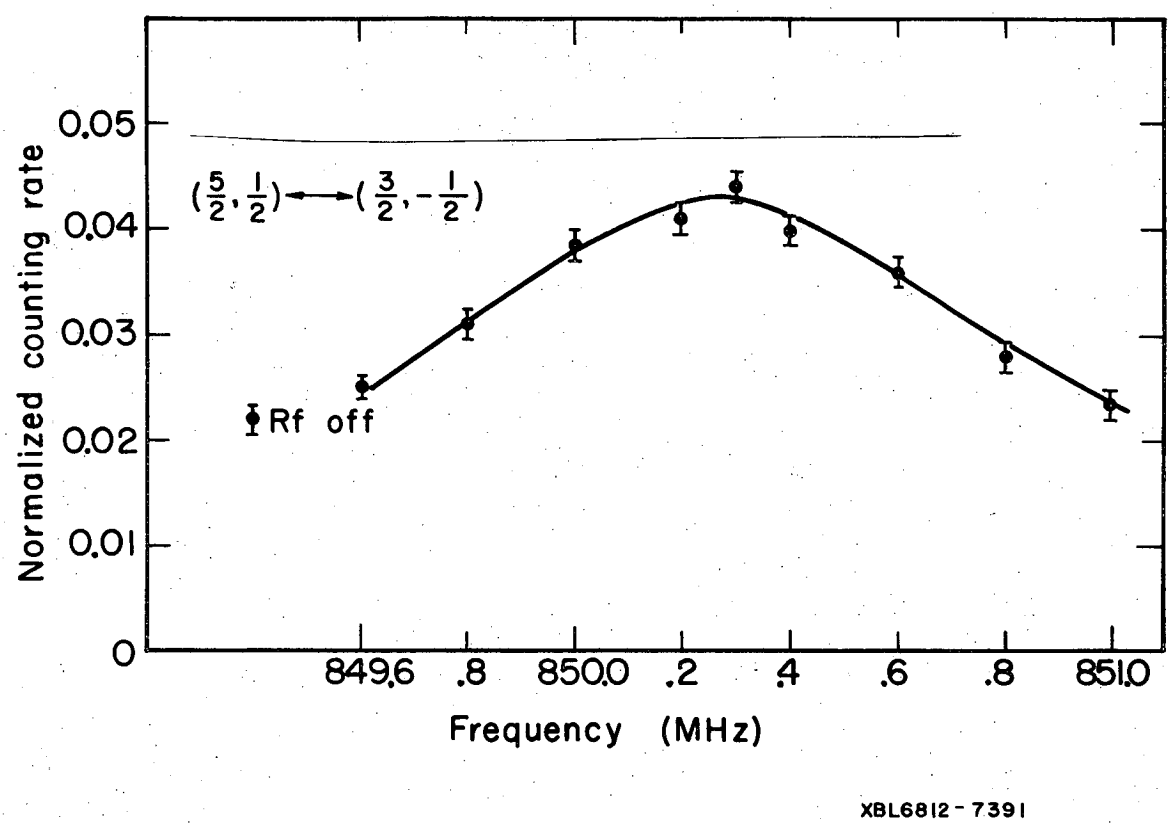

Fig. 17. $\Delta F=1$ transition in $^{75}Ge(^3P_2)$ at $\sim$5 gauss.

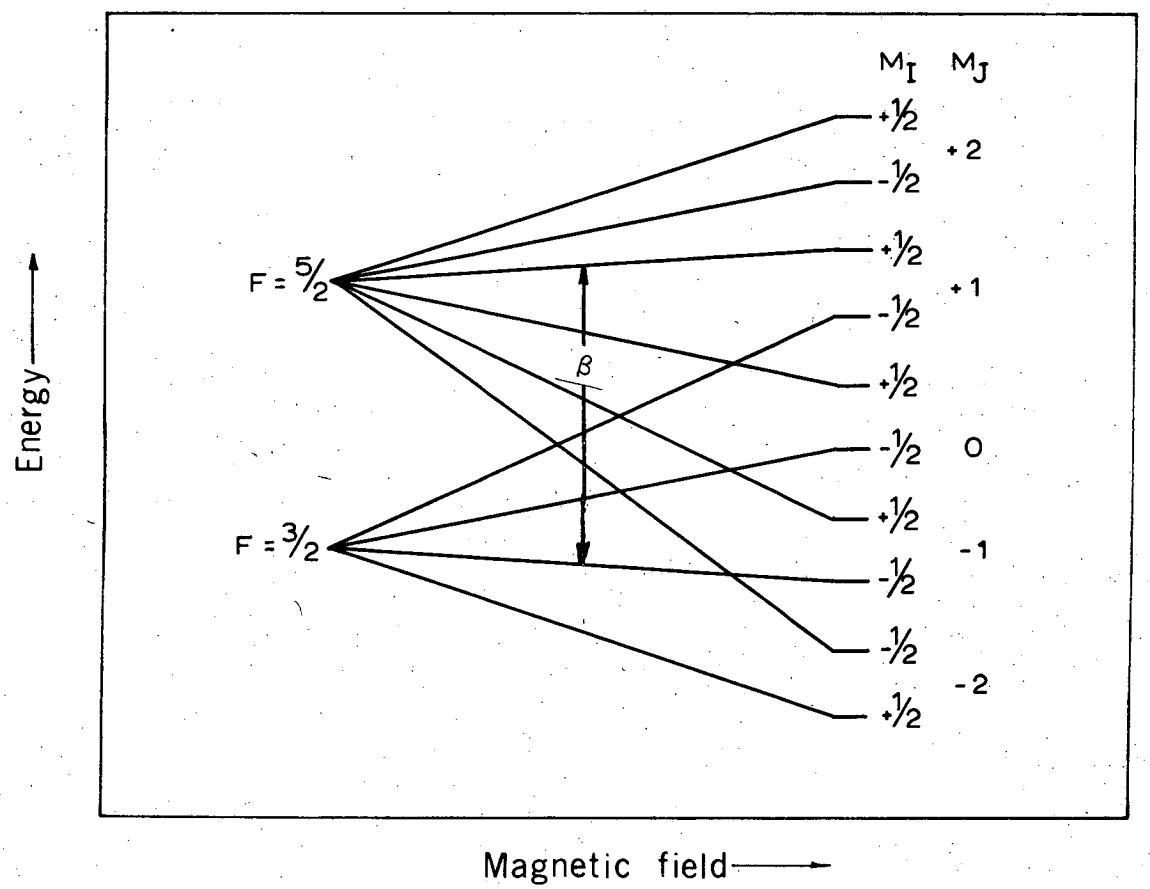

XBL 699 4903

Fig. 18. Schematic Breit-Rabi diagram for ^{75}Ge and ^{71}Ge in the $^3P_2$ state.

Table II. Observed resonances in ^{75}Ge, I = 1/2, J = 1.

Run No.	Calibration Isotope	Calibration Frequency (MHz)	Field (Gauss)	Ge^{75} Frequency (MHz)	Type*	Residuals (kHz)
975	^{85}Rb	.868(8)	1.858(18)	5.100(144)	α	-131
977	^{85}Rb	1.858(8)	3.968(17)	11.200(250)	α	-045
981	^{133}Cs	2.773(10)	7.908(29)	22.600(280)	α	-076
985	^{133}Cs	2.782(16)	7.935(46)	22.600(144)	α	-154
986	^{133}Cs	4.477(10)	12.752(28)	37.100(200)	α	-016
1001A	^{85}Rb	5.968(15)	12.661(32)	17.900(200)	γ	-014
1001B	^{85}Rb	5.968(15)	12.661(32)	18.900(200)	δ	-026
1001C	^{85}Rb	5.968(15)	12.661(32)	36.800(200)	α	-040
1006A	^{85}Rb	9.434(28)	19.904(58)	30.700(200)	δ	016
1006B	^{85}Rb	9.434(28)	19.904(58)	28.600(200)	γ	039
1007A	^{85}Rb	14.278(30)	29.890(61)	47.800(200)	δ	034
1007B	^{85}Rb	14.278(30)	29.890(61)	44.000(200)	γ	-017
1010A	^{85}Rb	24.250(20)	49.973(40)	84.400(200)	δ	077
1010B	^{85}Rb	24.250(20)	49.973(40)	78.100(200)	γ	-020
1011A	^{85}Rb	24.226(15)	49.926(30)	78.000(100)	γ	-035
1011B	^{85}Rb	24.226(15)	49.926(30)	84.150(100)	δ	-084
1012A	^{85}Rb	37.100(16)	74.955(31)	124.850(100)	γ	-108
1012B	^{85}Rb	37.110(10)	74.974(19)	132.300(100)	δ	-080
1014	^{85}Rb	.516(6)	1.104(13)	123.900(100)	β	-023
1094	^{85}Rb	.455(15)	.974(32)	123.650(50)	β	007
1119	^{85}Rb	50.515(15)	100.029(28)	450.400(100)	β	-015
1121	^{85}Rb	50.507(15)	100.015(28)	450.400(100)	β	039
1016	^{85}Rb	.979(6)	2.094(13)	126.050(50)	β	-003

*Transition types:

	F_1	M_1	F_2	M_2
α:	3/2	1/2	3/2	-3/2
γ:	3/2	1/2	3/2	-1/2
δ:	3/2	-1/2	3/2	-3/2
β:	3/2	1/2	1/2	-1/2

Table III. Results for ^{75}Ge in the $^{3}P_1$ state.

a (MHz)	μ_I (nm)	χ^2
-81.05(8)	+0.509(5)	2.28
+81.05(8)	-0.509(5)	3.30

Table IV. Observed resonances in ^{75}Ge; I = 1/2, J = 2.

Run No.	Calibration Isotope	Calibration Frequency (MHz)	Field (Gauss)	^{75}Ge Frequency (MHz)	Type*	Residuals (kHz)
1111A	^{85}Rb	.452(15)	.968(32)	841.900(200)	α	37
1111B	^{85}Rb	.936(200)	2.002(427)	843.800(200)	α	-235
1111C	^{85}Rb	2.337(15)	4.988(32)	850.400(100)	α	66
1111D	^{85}Rb	2.334(15)	4.981(32)	850.300(200)	α	-17
1111E	^{85}Rb	.961(15)	2.056(32)	844.000(200)	α	-148

*Transition type:

	F_1	M_1	F_2	M_2
α:	5/2	1/2	3/2	-1/2

Results: $a(^3P_2;^{75}Ge) = +335.94(9)$

$\chi^2 = 0.55$

Table V. hfs constants and nuclear moments of ^{73}Ge.

$^3P_1$	$^3P_2$
a = +15.5480(18)	-64.4270(7)
b = -54.566(9)	+111.825(13)
μ_I (^{73}Ge) = -0.8788	
Q_I = -0.285(1 ±0.15)	

(Refs. 16 & 28)

$\mu_I < 0$ and $\mu_I > 0$ is sufficiently pronounced to justify assigning a positive sign for μ_I.

On the basis of the known signs for μ_I and a for ^{73}Ge, therefore, we assign a negative sign for $a(^3P_1)$ and a positive sign for $a(^3P_2)$. This latter assignment is in agreement with the nonrelativistic LS coupling model, which predicts a positive sign for $a(^3P_2)$. What is more interesting is that the simplest LS model predicts $a(^3P_1) \equiv 0$, which is not in agreement with our experimentally measured value.

a. Origin of $a(^3P_1)$. Equation (19) gives a as

$$a = a_\ell \left[2-g + \frac{2(2L-n^2)}{n^2(2L-1)(2\ell+3)(2\ell-1)} \left\{ \frac{L(L+1)}{2J(J+1)} [J(J+1) + S(S+1) - L(L+1)] - \frac{3[J(J+1) - L(L+1) - S(S+1)][J(J+1) + L(L+1) - S(S+1)]}{4J(J+1)} \right\} \right] .$$

For the $4p^2\ ^3P_1$ state where

$$J = S = L = 1 \text{ and}$$

$$g = \text{Lande g factor} = -1.5,$$

$$a \equiv 0 \quad .$$

In Section II.B.3,4 two sources for this non-zero value of $a(^3P_1)$ were discussed. They are relativistic and configuration interaction effects.

The first effect can be estimated numerically from Eq. (45) using the listed values of $F_r(J, Z)$ in Kopfermann. This gives the relativistic correction a^r as

$$a^r = 21.6 \text{ MHz} \quad .$$

Detailed calculation is shown in the Appendices. The more accurate method of Sandars gives $a^r = -23.87$ MHz. The measured value a is

$$a = -81.05 \text{ MHz} \quad .$$

The difference between the measured value and the relativistic contribution must be assumed to be due to configuration interaction denoted by a^c:

$$a^c = a - a^r = \mp 81.05 + 23.87 = -57.18 \text{ MHz} \quad .$$

From Eq. (54a) similar contribution must be made to $a(^3P_2)$. So without configuration interaction

$$a(^3P_2) = a(^3P_2)_{measured} - a^c$$

$$= 335.945 - (-57.18) \text{ MHz}$$

$$= 393.12 \text{ MHz} \quad .$$

Calculation[29] with this value of a yields

$$\left\langle \frac{1}{r^3} \right\rangle_{av.} = 6.49 \; a_o^{-3} \quad .$$

This is to be compared with the value 5.7 a_o^{-3} which is derived from the atomic structure[27] $\xi = 904 \text{ cm}^{-1}$. It is interesting to note that if we neglect the effect of configuration interaction, $\left\langle \frac{1}{r^3} \right\rangle$ derived from $a(^3P_2)$ is 5.5 a_o^{-3}. This must be taken as fortuitous.

We take $\left\langle \frac{1}{r^3} \right\rangle = 6.49 \; a_o^{-3}$ as the correct value for the 4p electrons in Ge.

<u>b. Shell Model Comparison with Experiment for I, μ_I.</u> The measured spin I = 1/2 for ^{75}Ge is in complete agreement with the shell model predictions. It assigns the configuration $(1g_{9/2})^4(2p_{1/2})^1$, with J = 1/2 = I for 43 neutrons.

The Schmidt value for the magnetic dipole moment for the odd neutron is

$$\mu_I(\text{uncorr}) = +0.637 \text{ nm} \quad .$$

The measured value is

$$\mu_I(\text{uncorr}) = +0.509(5) \text{ nm} \quad .$$

The sign is predicted correctly and the magnitude is predicted to an accuracy of about 25%. This is not bad, considering the fact that the Schmidt values merely set limits to the values of the magnetic dipole moment.

C. ^{71}Ge ($^3P_2$)

A short experiment was performed to measure the hfs constant for the J = 2 state of ^{71}Ge. The main reason for undertaking this experiment was that we had trouble observing the J = 2,ΔF = 1 transition in ^{75}Ge. We thought that either our results for a(^{75}Ge; $^3P_1$) were wrong, or there was an hfs anomaly between ^{73}Ge and ^{75}Ge. If an anomaly did indeed exist, it would be much smaller for ^{71}Ge and ^{75}Ge because they both had spins of I = 1/2.

Previously, Goodman and Childs[27] had observed the $^3P_1$ ΔF = 1 transition very accurately in ^{71}Ge. In addition, they predicted a($^3P_2$) = 357±5 MHz based on their observations for ΔF = 0 transitions. We decided to measure this more accurately by observing the ΔF = 1, J = 2 transition. We found that, within our accuracy, the Fermi-Segrè formula held for ^{71}Ge and ^{73}Ge, so there was no detectable hfs anomaly.

Other results obtained by Goodman and Childs on ^{71}Ge were

$$I = 1/2, \quad a(^3P_1) = -87.05 \text{ MHz} \quad .$$

^{71}Ge has a half-life of 11 days. The isotope was produced by neutron irradiation of the 20% abundant stable ^{70}Ge isotope in the General Electric Test Reactor at Vallecitos. The neutron flux here was about 10^{14} neutrons/cm^{2}sec. Because of its half-life, ^{71}Ge is especially suitable for atomic beam work; it is possible to run for 1 to 3 weeks with a single bombardment. Several melted spheres of natural germanium were encapsulated in quartz. The first sample was irradiated for less than one week, and for this we only obtained a normalization count of about 400 counts/min., which was much lower than the bare minimum of 500 counts/min. required to see a good signal-to-background ratio. Subsequent bombardments were irradiated for 3 weeks, and excellent activity was then obtained.

1. Beam Formation

The procedure for beam formation was the same as for ^{75}Ge. About 3 days were allowed to pass so that the shorter-lived isotopes, ^{75}Ge and ^{77}Ge, could decay away. Again, tantalum ovens lined with carbon crucibles were used. For an electron bombardment power of about 160 watts, a normalization count of over 1500 count/min. was achieved. A satisfactory signal-to-background ratio of 3 was typical. ^{71}Ge was detected by its electron-capture x-rays. Thin (2 to 3 mm) crystals mounted on photomultipliers (RCA 6655A) were used to detect the subsequent gallium x-rays. The signals from the photomultipliers were fed to single-channel pulse-height analyzers set for the low-energy x-rays.

2. Results and Discussion

We started by verifying some of the results in Ref. 27. We observed the $\Delta F = 1$ transition for the $J = 1$ state. The frequency

for this transition was found to be in complete agreement with the predicted frequency based on the data in Ref. 27.

The Fermi-Segrè relation was used to compare ^{71}Ge with ^{75}Ge to obtain the value of $a(^3P_2)$. With this information, frequencies for the $\Delta F = 1$ transition at various magnetic fields were plotted. $\Delta F = 1$ transitions at 1, 2, 4, 5, and 8 gauss were observed. Figure 19 shows the resonance sweep at 1 gauss.

The data were analyzed in two ways. First our own $\Delta F = 1$ observations were separately fitted with the computer routine HYPERFINE. Secondly, our data were combined with the data of Goodman and Childs for the $\Delta F = 0$ transition and another fit was made. These data are listed in Table VI.

Both fits give the result

$$a(^3P_2\ ;\ ^{71}Ge) = +360.536(60)\ \text{MHz} \quad .$$

D. $^{69}Ge\ (^3P_1)$

1. Production

^{69}Ge has a half-life of about 38 hours. It was first identified in 1955 by Butement[30] through the cyclotron reaction $^{70}Ge\ (p,2n)\ ^{69}As \xrightarrow[\text{(15 minute)}]{} {}^{69}Ge$. It is the only isotope studied in this paper that cannot be produced by a reactor. ^{69}Ge can be produced by different cyclotron reactions:

(a) $^{66}Zn\ (\alpha,n)^{69}Ge$

(b) $^{69}Ga\ (d,n)^{69}Ge$

(c) $^{70}Ge\ (p,2n)^{69}As \xrightarrow[\text{(15 min.)}]{} {}^{69}Ge$.

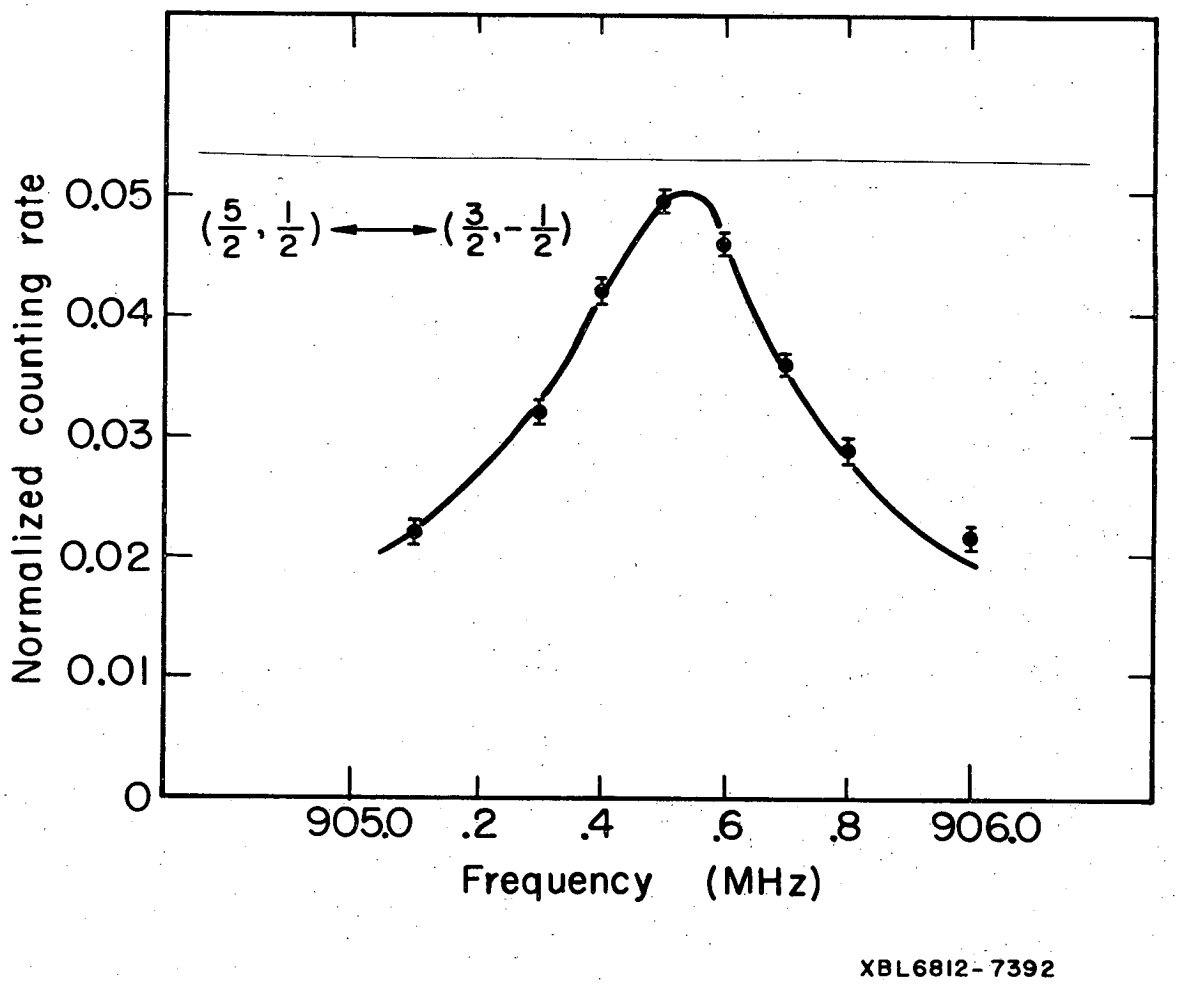

Fig. 19. $\Delta F=1$ transition in $^{71}Ge(^3P_2)$ at 1 gauss.

Table VI. Observed resonances in ^{71}Ge; I = 1/2, J = 2.

Run No.	Calibration Isotope	Calibration Frequency	Field (Gauss)	Ge^{75} Frequency	Type†	Residuals (kHz)
GC 5 *	^{133}Cs	24.958	70.006	236.666(5)	α	- 25
GC 4 *	^{133}Cs	18.450	52.004	175.300(6)	α	- 0.1
GC 3 *	^{133}Cs	13.789	39.003	131.200(15)	α	- 9
GC 2 *	^{133}Cs	7.035	20.001	67.100(25)	α	- 2
GC 1 *	^{133}Cs	.350	1.000	4.896(15)	α	-126
1086	^{85}Rb	.463(15)	.991(32)	903.400(200)	β	- 16
1087	^{85}Rb	.869(58)	1.859(124)	905.300(200)	β	62
1088	^{85}Rb	1.863(15)	3.979(32)	909.800(200)	β	98
1116	^{85}Rb	1.815(15)	3.877(32)	909.500(100)	β	14
1117	^{85}Rb	.451(15)	.966(32)	903.400(100)	β	37
1118A	^{85}Rb	.946(15)	2.024(32)	905.500(100)	β	- 83
1118B	^{85}Rb	.941(15)	2.013(32)	905.550(50)	β	- 11

* From the work of Goodman and Childs (Ref. 27).

† Transition types:

	F_1	M_1	F_2	M_2
α	5/2	1/2	5/2	-3/2
β	5/2	1/2	3/2	-1/2

Table VI A. Results for ^{71}Ge in the $^3P_2$ State Using our $\Delta F = 1$ Transitions Alone.

a (MHz)	μ_I (uncorr.)	χ^2
-360.54(6)	-0.546(5)	0.47
+360.54(6)	+0.546(5)	0.47

Table VI B. Results for ^{71}Ge in the $^3P_2$ state using the combined data of our $\Delta F = 1$ transitions and $\Delta F = 0$ transitions from Goodman and Childs.

a (MHz)	μ_I (uncorr.)	χ^2
+360.54(6)	+0.546(5)	0.56
-360.54(6)	-0.546(5)	0.63

From Refs. 27 and 16:

a = +357(5) MHz.
μ_I(uncorr.) = +0.546.

Methods (a) and (b) were first considered. However, to obtain Ge metal by both of these methods requires an extensive and complicated chemical separation and reduction of about four hours duration. Since ^{69}Ge emits strong γ-radiations in its decay, one should have as little exposure as possible to the radiations. For these reasons, we decided to try the third method. Chemical separation of ^{69}Ge from the other radioactive As isotopes by this reaction can be avoided by taking advantage of the difference in the vapor pressures of Ge and As. The method of achieving this will be discussed fully in the next section. The drawbacks of this method will also be discussed.

Ingots of natural germanium metal were sliced into discs about .078 in. thick. This thickness degraded the bombarding proton energy of 37 MeV to about 20 MeV, covering most of the energy range for the ^{70}Ge (p,2n)^{69}As reaction. The cross-section for this reaction was not known. We first tried .090 in. discs, but these were not satisfactory because the sample invariably became hot, burnt, and oxidized. Hence, we settled on the above size, although 90 mils would have completely covered the energy range. Secondly, we also wanted to maximize the specific activity of $^{69}Ge(^{69}As)$ as compared with other numerous As isotopes simultaneously produced.

Both the Berkeley 88" cyclotron and the 76" cyclotron at Davis were used. At the 88" cyclotron, current of up to 27 μA was used, while at Davis the average cyclotron current was about 15 μA. In both cases, a total charge of about 300 μA-hr was found necessary to obtain a reasonable amount of activity.

2. Beam Formation

On delivery from the cyclotron, targets were usually allowed to sit for at least 2 hours. This permitted the parent isotope, ^{69}As, to decay through about eight half-lives. Some of the sitting time was used in breaking and pulverizing the germanium piece in the lead-shielded cave. The powder was then loaded into four or five outgassed ovens. The ovens were of the same design as the ones used for the other Ge isotopes.

Once loaded into the atomic-beam machine, the heating was done in steps. The purpose of the procedure was to drive away the arsenic isotopes. Arsenic has a vapor pressure of 1 mm at about 700°C, whereas it takes 1500°C for germanium to reach 1 mm vapor pressure.

The oven power was progressively increased from 50 watts to that required for normal Ge runs – usually about 150 watts. It took about 30 minutes to achieve this. The drawback to this method was probably that much of the arsenic merely settled on the cooler part of the oven-loader. Once the oven became hotter, the arsenic reevaporated, thereby acting as a broad source. In this way, it contributed heavily to the background. With pure germanium isotopes, a normalized background for no rf of .05 was achieved for an oven chamber pressure of about 2×10^{-6} torr. For ^{69}Ge runs, the normalized background ratio sometimes rose to about .2. On a few occasions when we ran three or four times without cleaning the oven chamber, it usually became almost impossible to see a signal. Perhaps, if one had to do it over again, a chemical separation should be strongly recommended. In the long run, it might have saved a lot of time.

This problem was compounded on those several occasions when the targets were burnt. Initially, the germanium discs were too thick. They heated quickly on the front surface and the cooling at the back surface was not fast enough to conduct away the generated heat. These targets were burnt. For the first two Davis targets, there were also leakages in the cooling system, which also produced burnt targets. At the 88" cyclotron, high running currents and total power concentrated in a small spot on the target were probably responsible for the burning of the sample.

The above reasons may justify the poorer signal-to-background ratios of ^{69}Ge when compared to the ones for ^{75}Ge and ^{71}Ge.

^{69}Ge decays by emitting positrons. Therefore, Geiger β-counters were employed for its detection. The setup has already been sketched in Fig. 7. On days when we obtained good, unburnt targets, normalization counts of 1000 counts/min. were easily observed for oven power of about 150 watts. Just as for the previous isotopes, the minimum normalization count seemed to be about 500 cpm in order to observe a decent signal.

3. Spin Measurement

Precisely the method described for measuring the spin of ^{75}Ge was followed. The result of the spin search at 1 gauss is shown in Fig. 20. Although the error bar on each point was large and the background, as explained earlier, was high, the I = 5/2 signals were significantly above the background, as indicated by the points I = 5/2, J = 1 and I = 5/2, J = 2. At this field, the I = 3/2, J = 1 state had the same predicted frequency as the I = 5/2, J = 2 state. Hence, to

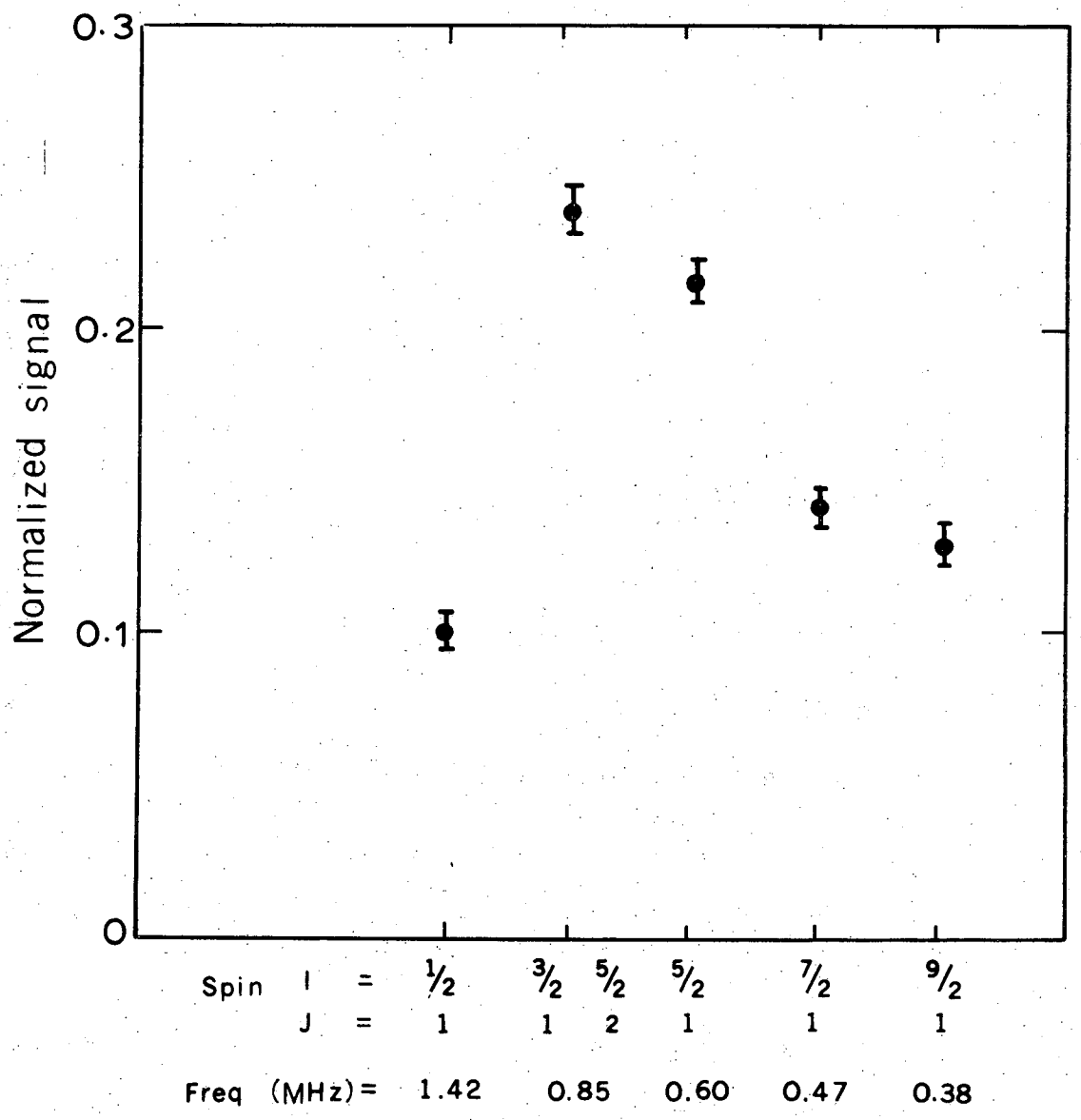

XBL 699 4906

Fig. 20. ^{69}Ge spin search at 1 gauss.

determine the spin without ambiguity, it was necessary to go to a higher field where there was enough separation between these two cases. $\Delta F = 0$ resonance sweeps were then made at 3 gauss for both $J = 1$ and $J = 2$ state. The result, as shown in Fig. 21, unequivocably confirmed the assignment of spin $I = 5/2$ to ^{69}Ge.

Two further steps were taken to confirm the spin assignment. First, a decay analysis was made. The 38-hr half-life obtained identified the isotope as ^{69}Ge. This is illustrated in Fig. 22. Secondly, the γ-ray spectrum shown in Fig. 23 was taken with a Ge (Li) detector. The ^{69}Ge peaks can easily be identified and were found to be in agreement with the spectrum in Ref. 31. In Fig. 23 peaks also are visible which definitely belong to some arsenic isotopes.

4. Hyperfine Structure Measurement

The steps taken in Section IV. B.4. for ^{75}Ge were carried out for ^{69}Ge. The $\Delta F = 0$ double quantum transition labelled α in the hfs diagram, Fig. 24, was followed up to 25 G. A computer fit of all the observations for this transition at various C-fields yielded a value of a with an uncertainty of about 0.7 MHz. A trial search for one $\Delta F = 1$ transition at 25 G was decided upon. The expected transition probability had its highest values at this field. Figure 25 is the result of the search for the upper $\Delta F = 1$ transition, labelled β in the hfs diagram.

The $(F = 7/2 \leftrightarrow F = 5/2)$ transition interval observed in Fig. 25 has the a and b dependence given by

$$h\nu_1 = E_{hfs}\ (5/2) - E_{hfs}\ (7/2) = \frac{7a}{2} + \frac{21}{20}\,b \quad . \qquad (65)$$

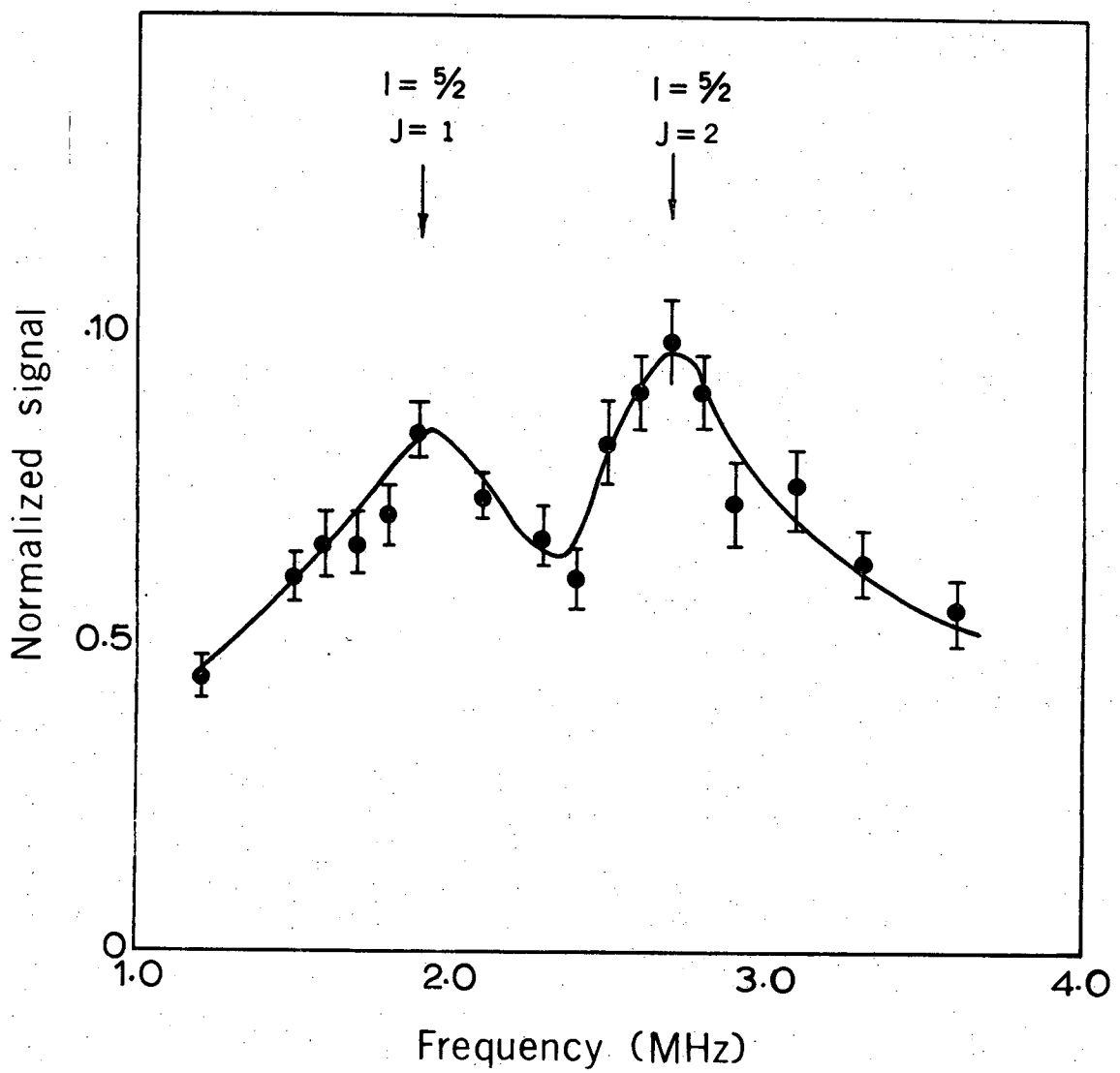

XBL 699 4907

Fig. 21. ^{69}Ge confirmation of I=5/2 at 3 gauss.

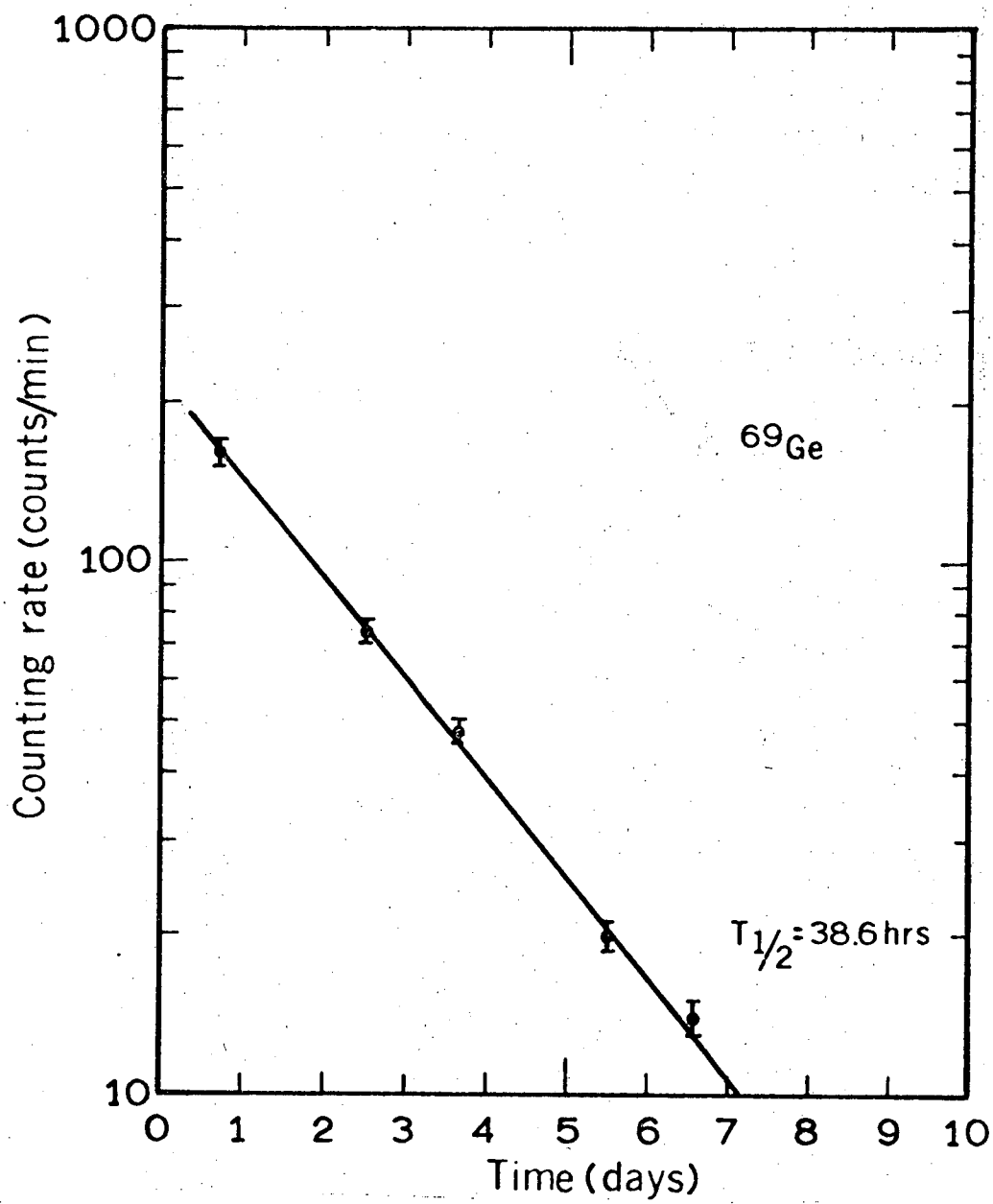

XBL 699 4908

Fig. 22. Decay of activity on I=5/2 button from ^{69}Ge.

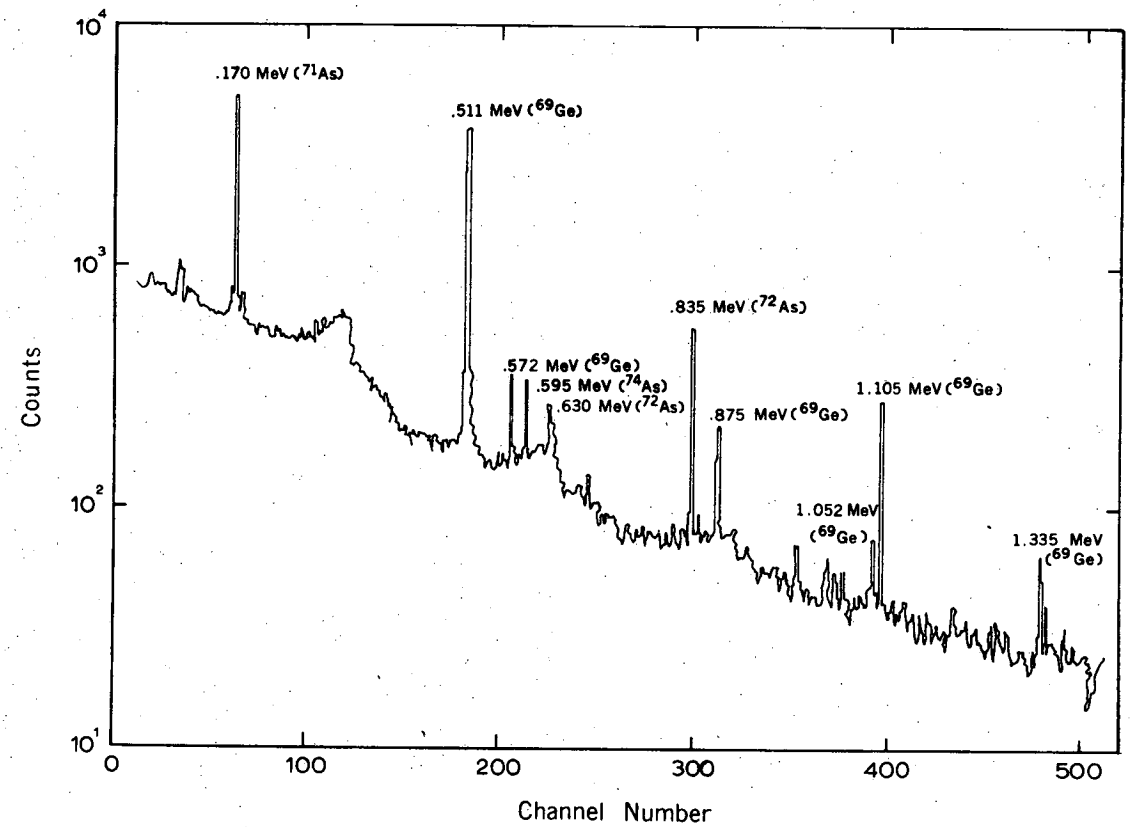

XBL 699 4909

Fig. 23. γ-ray spectrum of unheated ^{69}Ge produced by the 76" cyclotron at Davis.

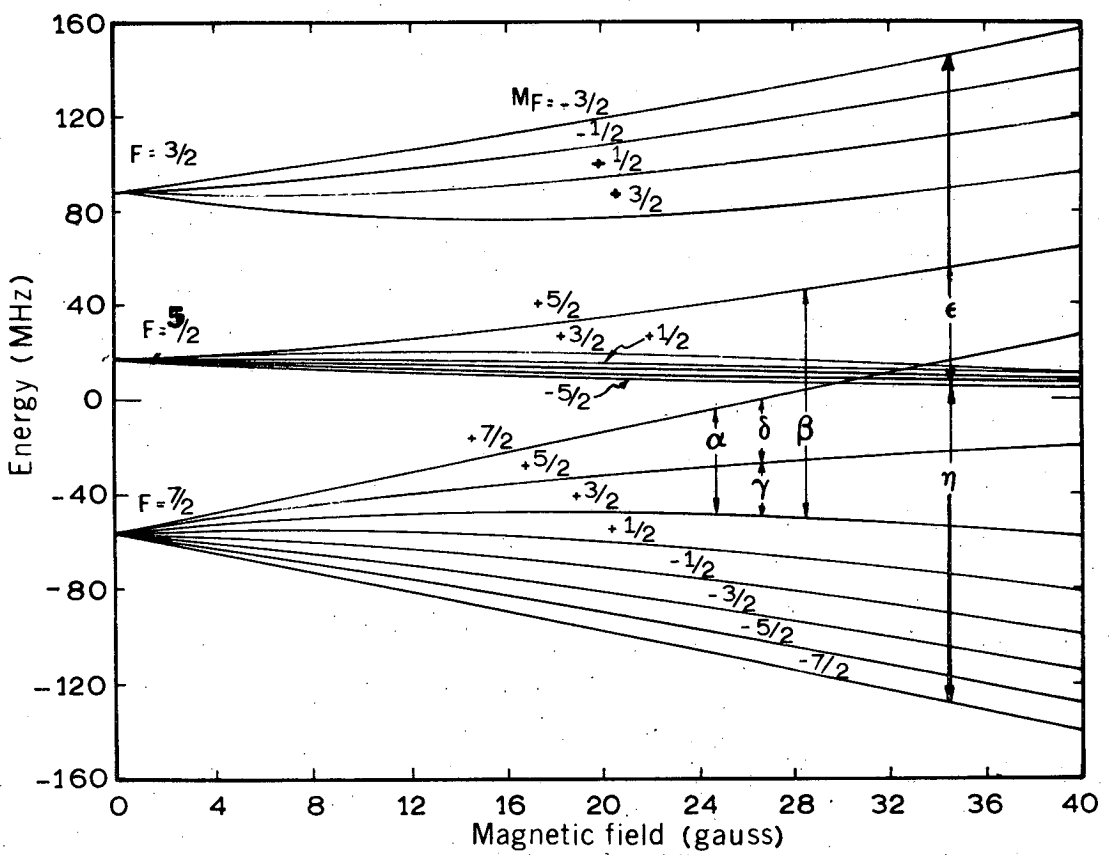

XBL 699 4911

Fig. 24. Energy level diagram for the $^3P_1$ hfs levels of 38-hr ^{69}Ge with a<0, b>0.

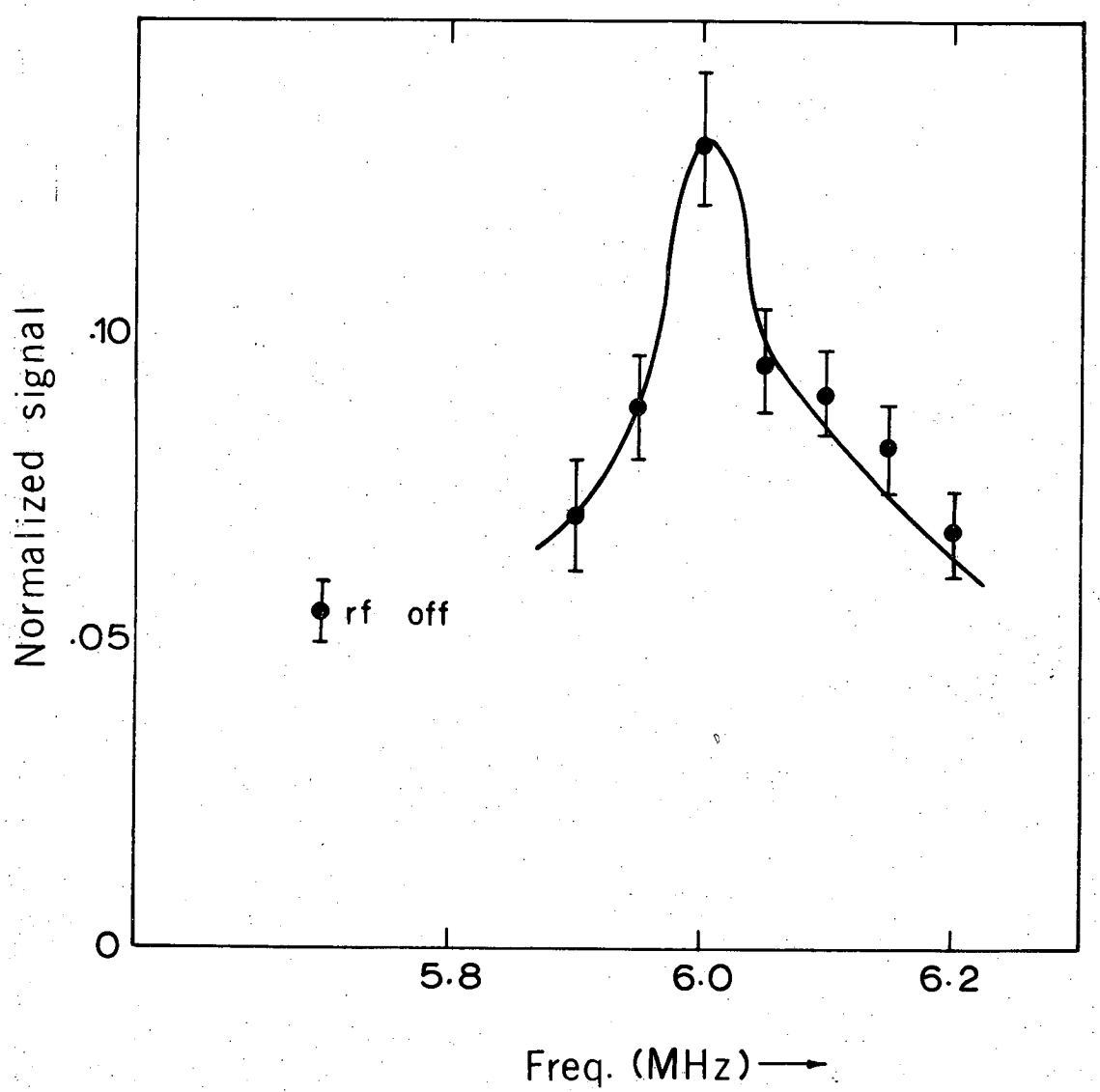

XBL 699 4910

Fig. 24a. ^{69}Ge $\Delta F=0$, $\Delta M_F=2$ at 9 gauss. (3.5, 1.5)↔(3.5, 3.5).

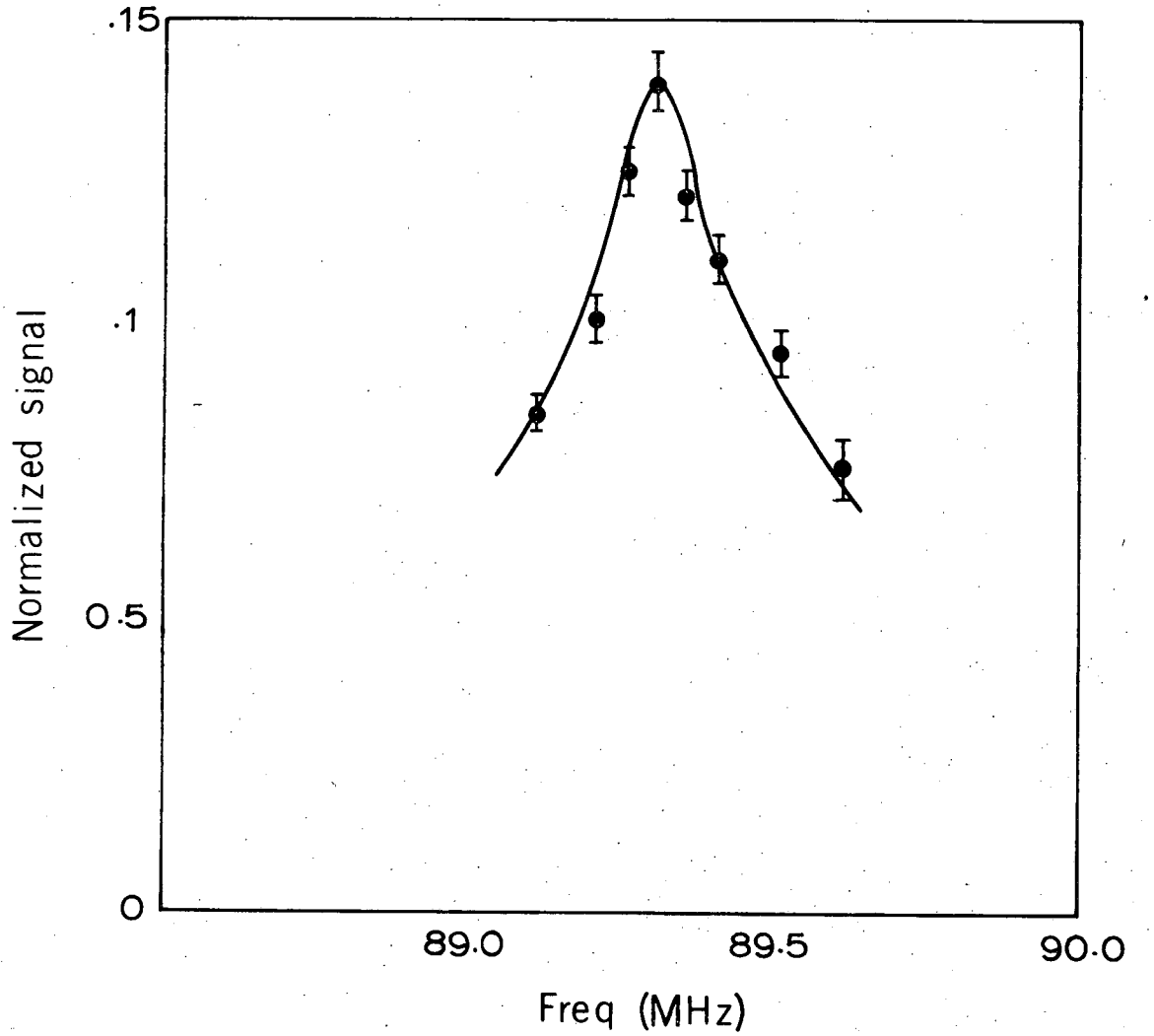

XBL 699 4912

Fig. 25. ^{69}Ge $\Delta F=1$ transition at 25 gauss. (2.5, 2.5)↔(3.5, 1.5).

The observation of $h\nu_1$ merely fixed the lefthand side of the above equation; hence, it yielded only one equation for a and b. The determination of the second hyperfine-interval would similarly yield another equation in a and b given by

$$h\nu_2 = E_{hfs}\ (3/2) - E_{hfs}\ (5/2) = \frac{5}{2}\,a - \frac{3}{2}\,b \quad . \tag{66}$$

Therefore, the next step was to measure the second hyperfine interval. The $(F = 3/2 \leftrightarrow F = 5/2)$ transition violates the machine selection rule and therefore could not be observed directly. But even after the observation of the $\Delta F = 1$ transition, the uncertainties in a and b were still too large to make a search for a two-frequency $\Delta F = 1 + \Delta F = 1$ transition feasible. In order to lower these uncertainties, we returned to the $\Delta F = 0$ transition. This time, the two-frequency technique was employed. The transitions involved were δ and γ, i.e., $(7/2,\ 3/2) \leftrightarrow (7/2,\ 5/2)$ and $(7/2,\ 5/2) \leftrightarrow (7/2,\ 7/2)$. One of the transitions, $(7/2,\ 3/2) \leftrightarrow (7/2,\ 5/2)$, depends upon the interval $(F = 5/2 \leftrightarrow F = 3/2)$. It therefore would yield more information about the second interval $h\nu_2$. The uncertainty in the γ-transitions was much smaller than the δ-transition, so the former was kept constant and the latter was varied until a resonance was obtained. This was carried out at 69 gauss. The new observation along with the earlier ones narrowed the uncertainty in $h\nu_2$ to about 0.5 MHz.

It was then measured by the two-frequency technique. The resonances were observed by making one rf field connect the levels $(F = 7/2 \leftrightarrow F = 5/2)$ while the other connected the $(F = 5/2 \leftrightarrow F = 3/2)$

levels. The transitions so selected are labelled η and ε in Fig. 24. Figure 26 shows the resonances obtained at 10 gauss. Figure 27 is the $\Delta F = 1$ ($F = 7/2 \leftrightarrow F = 5/2$) transition at 4 gauss, its field-independent point.

With the two hfs intervals measured, a and b were uniquely determined in magnitude. A least-squares fit (by the computer routine HYPERFINE) of frequencies to the 27 observed resonances varying a and b yielded the results given in Tables VII and VIII along with the χ^2 of the fits.

5. Results and Interpretations

The Fermi-Segrè relation was used to compare ^{69}Ge with ^{73}Ge. The results for ^{69}Ge are listed in Table VIII.

The numbers in parentheses indicate the error in the least significant figure, and in the case of a and b represent two standard deviations. For μ_I, the error of 1% allows for a possible hfs anomaly, while the error of 20% for Q_I(uncorr) is not a measure of the precision of the experimental determination, but results from the theoretical problem of extracting Q from b. This point will be discussed in fuller detail in the next section. We have made no diamagnetic correction for μ_I(uncorr) nor the Sternheimer shielding correction for Q.

The difference in χ^2 for the $\pm\mu$ fits is not pronounced enough to choose one. But from our work, a positive sign was measured for $\mu_I(^{75}\text{Ge})$, while a negative sign[27] was measured for $\mu_I(^{73}\text{Ge})$. In both cases, μ_I(uncorr) and a have opposite signs. So we expect $\mu_I(^{69}\text{Ge})$ and $a(^3P_1, {}^{69}\text{Ge})$ to have opposite signs. Q_I and b are known to have

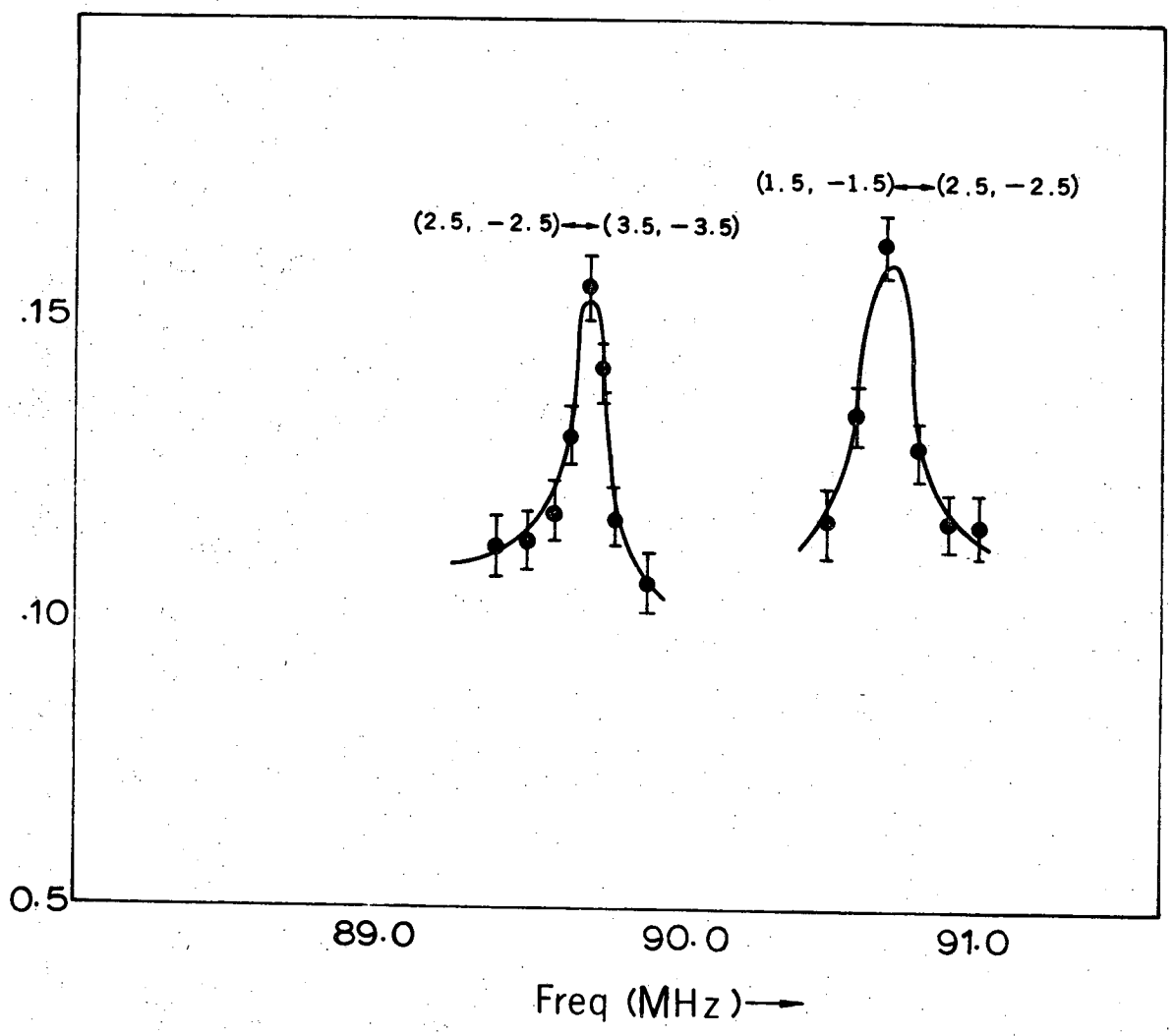

XBL 699 4913

Fig. 26. ^{69}Ge, $\Delta F=1 + \Delta F=1$ transitions at 10 gauss.

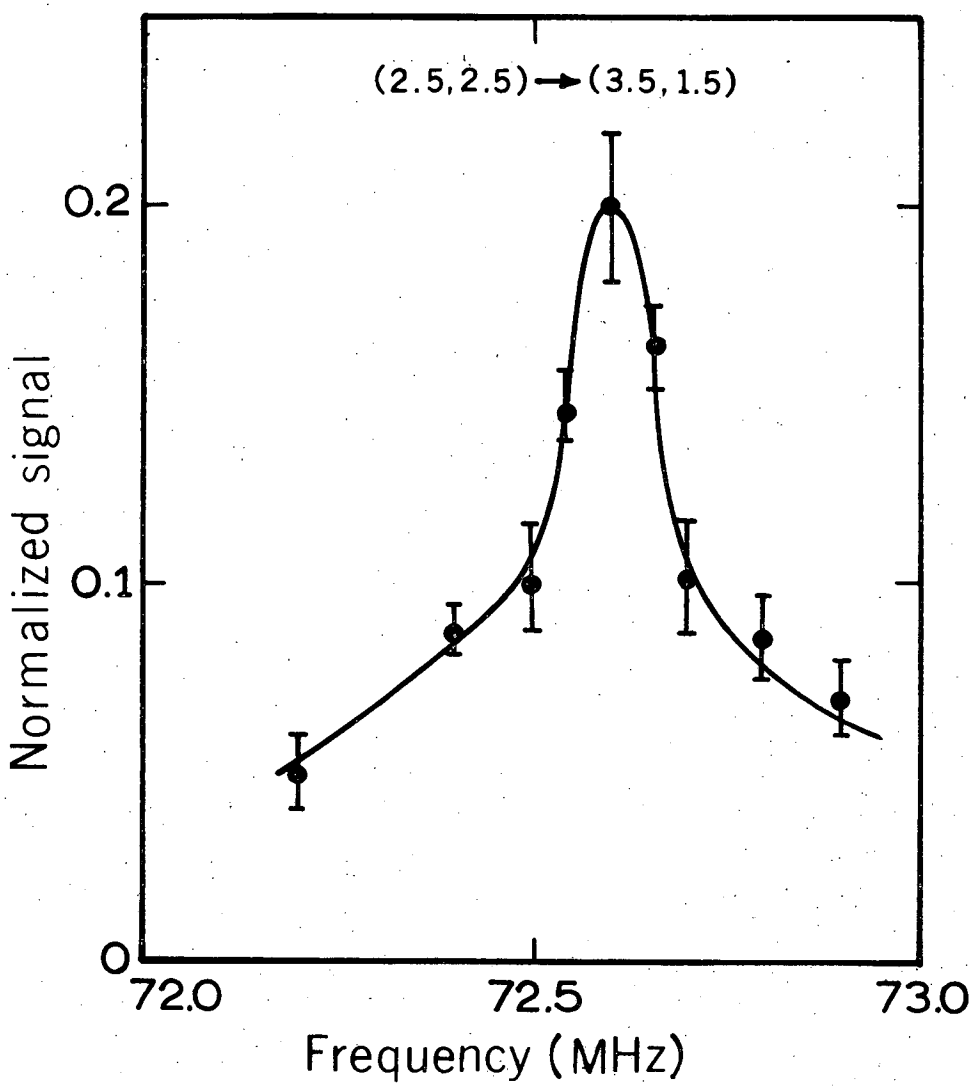

XBL 699 4914

Fig. 27. ^{69}Ge $\Delta F=1$ transition at its field-independent point ∿4.3 G.

Table VII. Observed resonances in ^{69}Ge; I = 5/2, J = 1.

Run No.	Calibration Isotope	Calibration Frequency (MHz)	Field (Gauss)	^{69}Ge Frequency (MHz)	Type*	Residuals (kHz)
1126	^{85}Rb	.469(20)	1.004(42)	1.200(100)	α	-26
1135	^{133}Cs	1.069(20)	3.053(57)	3.800(100)	α	-59
1140	^{133}Cs	2.083(30)	5.945(85)	7.800(200)	α	-90
1140A	^{133}Cs	2.779(20)	7.925(57)	10.800(200)	α	-69
1141	^{133}Cs	2.458(20)	7.011(57)	9.500(100)	α	28
1141A	^{133}Cs	1.675(20)	4.780(57)	6.200(100)	α	-22
1141B	^{133}Cs	2.470(20)	7.048(57)	9.600(100)	α	73
1142	^{133}Cs	3.096(20)	8.829(57)	12.200(100)	α	-90
1142A	^{133}Cs	3.064(20)	8.737(57)	12.100(100)	α	-44
1143	^{133}Cs	3.849(20)	10.970(57)	15.800(100)	α	-12
1146	^{133}Cs	5.149(30)	14.659(85)	22.400(100)	α	-4
1153	^{133}Cs	5.319(20)	15.143(57)	23.300(100)	α	-20
1153A	^{133}Cs	6.373(20)	18.126(57)	29.200(100)	α	-25
1156	^{133}Cs	8.812(20)	25.018(56)	44.600(100)	α	-19
1157	^{133}Cs	8.836(30)	25.087(85)	24.200(200)	δ	-297
1157A	^{133}Cs	8.836(30)	25.087(85)	20.500(300)	γ	213
1163	^{133}Cs	8.760(20)	24.872(56)	89.300(100)	β	-124
1168	^{133}Cs	24.677(20)	69.234(55)	89.100(100)	γ	89
1172	^{133}Cs	3.577(25)	10.196(71)	90.700(100)	ε	-1
1172	^{133}Cs	3.577(25)	10.196(71)	89.800(100)	η	74
1172	^{133}Cs	3.556(18)	10.137(51)	90.600(100)	ε	18
1173	^{133}Cs	3.577(20)	10.196(57)	89.600(100)	η	-25
1174	^{133}Cs	8.803(20)	24.993(56)	20.200(100)	γ	11
1174B	^{133}Cs	8.813(30)	25.022(85)	89.400(100)	β	-275
1175B	^{133}Cs	1.488(20)	4.248(57)	72.600(100)	β	58
1178	^{133}Cs	1.550(20)	4.425(57)	72.550(500)	β	78
1180	^{133}Cs	1.507(20)	4.303(57)	79.100(100)	ε	7

*Transition types:

	F_1	M_1	F_2	M_2		F_1	M_1	F_2	M_2
α:	7/2	7/2	7/2	3/2	δ:	7/2	7/2	7/2	5/2
β:	5/2	5/2	7/2	3/2	ε:	3/2	-3/2	5/2	-5/2
γ:	7/2	5/2	7/2	3/2	η:	5/2	-5/2	7/2	-7/2

Table VIII. Results for ^{69}Ge in the $^3P_1$ state.

a (MHz)	b (MHz)	μ_I(uncorr) (nm)	Q_I(uncorr) (barns)	χ^2
-23.39(3)	+8.28(8)	+0.733(7)	+0.043(8)	7.97
+23.39(3)	-8.28(8)	-0.733(7)	-0.043(8)	8.14

positive signs for ^{73}Ge from Ref. 27, and since b/a is negative for ^{69}Ge, b($^3P_1$, ^{69}Ge) will therefore have a positive sign, the same as does Q_I.

a. Origins of a($^3P_1$). Because the electronic effects in ^{75}Ge and ^{69}Ge are similar, we can only offer similar explanations for the non-zero value of a. These are relativistic and configuration interaction effects.

We will use Eq. (45) and Eq. (54) to calculate the relativistic effect. The result is

$$a^{rel} = -6.88 \quad .$$

The difference between the observed a = -23.39 MHz and a^{rel} will be assumed to be due to configuration interaction:

$$a^c = a - a^{rel}$$

$$= -16.51 \text{ MHz} \quad .$$

Configuration interaction, therefore, will be assumed to contribute about 73% of the hfs constant a($^3P_1$) for ^{69}Ge. This is the same fraction it contributes to a($^3P_1$) for the other isotopes ^{75}Ge and ^{71}Ge, and follows directly from the method of computing a.

b. The Nuclear Quadrupole Moment. If we employ the Fermi-Segrè relation to compare ^{69}Ge with ^{73}Ge, the result for Q_I(^{69}Ge) is

$$Q_I(\text{uncorr}) = \pm 0.043(8) \text{ barn} \quad .$$

A relativistic calculation using Eq. (47) and the correction factor listed at the back of Ref. 12 gives

$$Q_I(\text{uncorr}) = \pm 0.042(8) \text{ barn} \quad .$$

Thus, relativistic effects contribute only about 2%. The effects of configuration interaction have not been considered in the above calculations. This is probably very important but is very difficult to evaluate reliably. We need to know the a values of more than one state before we can calculate the type of configuration corrections given by Eq. (50). Also not considered are the Sternheimer shielding corrections. The angular part of this alone for $4p^2$ electrons was calculated to be about 4%.[16] On these accounts, we have assigned an error of about 20% for our lack of knowledge of the proper theoretical treatment of the experimental data.

c. Comparison of Measured Value of I, μ_I with Shell Model. The measured spin I = 5/2 for the ground state of 37-hr ^{69}Ge is in agreement with the shell model assignment of the $1f_{5/2}$ sub-shell to the 37th odd neutron.[31] In addition, a spin of 5/2 has also been predicted for ^{69}Ge based on the β-decay of the ground state of ^{69}Ge to the ground state of ^{69}Ga.[32] ^{67}Zn with 37 neutrons was predicted to have the same neutron configuration. It, too, has a measured spin of 5/2.

The Schmidt value for the magnetic moment of a $1f_{5/2}$ odd neutron is +1.36 nm. The value calculated by Migdal,[23] using the quasi-particle method, is 0.90 for ^{67}Zn for this configuration. It is in better agreement with the observed value of ±0.733(7) for ^{69}Ge. A positive sign is thus predicted for μ_I, and the sign of a should be negative. Our results were not sufficiently precise to verify this.

The quadrupole moment predicted by the single particle shell model is +0.0005 barns. Migdal's calculation yields the corrected value $Q_I(^{69}Ge) = +0.11$. The observed uncorrected value is 0.043(8). In Ref. 32, on the basis of the $(1f_{5/2})^5$ configuration assignment to the ground state of ^{69}Ge, a very small and positive quadrupole moment was predicted. Migdal, too, predicts a positive value. On this basis, we expect a positive value for Q and, by comparison with ^{73}Ge, a positive value for $b(^3P_1)$ also.

While the shell model explains the nuclear spin assignments of the Ge isotopes, it needs drastic modification to explain the measured electromagnetic moments. In this case, the quasi-particle theory of Migdal seems to be in better agreement with experimental values of the Ge nuclear moments than the shell model.

ACKNOWLEDGMENTS

Many people have rendered invaluable help and encouragement in the course of this work.

In particular, my special thanks and deepest respect go to my research director, Professor H. A. Shugart, for introducing me to atomic beam research and the atomic beam group.

It has been my good fortune and pleasure to be associated with Dr. S. G. Schmelling during the entire period of the investigations. I am deeply indebted for his patience in teaching me the experimental techniques, and discussions with him during all phases of the work were invaluable.

I would also like to thank the following:

All the good, helpful members of the Atomic Beam Group.

The Health Chemistry group, in particular, Mr. Ed Heilstad and Mr. Gene Russel for assistance in handling the radio-isotopes and in scheduling targets.

Mrs. Jean Atteridge and Miss Nadine Kamada, for typing this paper.

Mr. Pat Yarnold for many hours of counting radio-active samples.

The African-American Institute for financial support during my entire graduate studies.

This research was supported by the U. S. Atomic Energy Commission.

APPENDICES

A. Relativistic Correction Factors

The $P^{(k_s k_\ell)k}$ of Eq. (54b) for $k = 1$ are given by

$$P^{(10)1} = \frac{4\mu_o}{3(2\ell+1)}\sqrt{\frac{6}{(2\ell+1)}}\,[\ell(\ell+1)\,F_{++} - \ell^2(\ell+1)\,F_{--} - \ell(\ell+1)\,F_{+-}]$$

$$P^{(12)1} = \frac{2\mu_o(\ell+1)}{(2\ell+1)(2\ell+3)(2\ell-1)}\sqrt{\frac{5\ell(2\ell+3)(2\ell-1)}{3(\ell+1)(2\ell+1)}} \times$$

$$[-4\ell(\ell+1)(2\ell+1)\,F_{++} + 4\ell(\ell+1)(2\ell+3)\,F_{--} - (2\ell+3)(2\ell-1)\,F_{+-}]$$

$$P^{(01)1} = \frac{4\mu_o}{(2\ell+1)}\sqrt{\frac{\ell(\ell+1)}{2(2\ell+1)}}\,[2\ell(\ell+1)\,F_{++} + 2\ell(\ell+1)\,F_{--} + F_{+-}]$$

where the F's are given by

$$F_{jj'} = \frac{-2}{\alpha a_o\,(K+K'+2)}\int_o^\infty (PQ' + QP')r^{-2}\,dr \quad .$$

The + or - signs are written for j and j' according to whether they are $\ell \pm 1/2$; $K = -(j + 1/2)$ for $j = \ell + 1/2$ and $K = j + 1/2$ for $j = \ell - 1/2$.

P and Q are the relativistic radial wave functions α and a_o are the fine-structure constant and Bohr radius.

The F's may be determined by using $\langle r^{-3}\rangle$ from Eq. (29) multiplied by appropriate correction factors obtained from tables at the back of Kopfermann's Nuclear Moments, Ref. 12. The various $\langle r^{-3}\rangle$ of Eq. (54d) are given by

$$\langle r^{-3}\rangle_{01} = \frac{1}{(2\ell+1)^2}\,[2\ell(\ell+1)\,F_{++} + 2\ell(\ell+1)\,F_{--} + F_{+-}]$$

$$\langle r^{-3}\rangle_{12} = \frac{1}{3(2\ell+1)^2}\,[-4\ell(\ell+1)(2\ell-1)\;F_{++} + 4\ell(\ell+1)(2\ell+3)\;F_{--} - (2\ell+3)(2\ell-1)\;F_{+-}]$$

$$\langle r^{-3}\rangle_{10} = \frac{4}{3}\;\frac{\ell(\ell+1)}{(2\ell+1)^2}\,[(\ell+1)\;F_{++} - \ell\;F_{--} - F_{+-}] \quad .$$

Integral	Factor (Kopfermann)
F_{--}	$-F''$
F_{++}	$-F'$
F_{+-}	$-G$.

B. Relativistic Contribution to $a(^3P_1)$ in ^{75}Ge

The relativistic contribution a^r was calculated by using the effective operator $H_{hfs\ eff.}$ of Eq. (54d) and the formulas in Appendix A. a^r is given by

$$a^r = a^r_{01} + a^r_{12} + a^r_{10}$$

where a^r_{01} is the contribution due to the term in $\vec{\ell}$ and a^r_{12} that due to the $(\vec{s}\,\vec{C}^{(2)})^{(1)}$ term and a^r_{10} that due to the $\vec{s}$ term in Eq. (54d).

In this calculation, we use $\langle r^{-3}\rangle$ determined by Goodman and Childs (Ref. 16) for ^{73}Ge with $Z_{eff} = 32-4 = 28$.

From Ref. 12

$$F_{--} = 1.0818$$

$$F_{+-} = 1.0185$$

$$F_{++} = 1.0166 \quad .$$

The matrix elements of the individual operators are

$$\langle p^2\ {}^3P_1 || \sum \vec{\ell}_i || p^2\ {}^3P_1\rangle = \sqrt{3/2}$$

$$\langle p^2\ {}^3P_1 || \sqrt{10}\ \sum (\vec{s}_i \vec{C}^{(2)})^{(1)} || p^2\ {}^3P_1\rangle = \sqrt{3/2}$$

$$\langle p^2\ {}^3P_1 || \sum \vec{s}_i || p^2\ {}^3P_1 \rangle = \sqrt{3/2} \quad .$$

$$\langle r^{-3} \rangle_{01} = 1.0458$$

$$\langle r^{-3} \rangle_{12} = 1.1128$$

$$\langle r^{-3} \rangle_{10} = -0.0199$$

$$\langle r^{-3} \rangle = 6.7\ a_o^{-3} \quad \text{(Ref. 16)} \quad .$$

The results are

$$a^r_{01} = +\ 287.60 \text{ MHz}$$

$$a^r_{12} = -306.02 \text{ MHz}$$

$$a^r_{10} = -5.47 \text{ MHz}$$

$$a^r = -23.87 \text{ MHz} \quad .$$

For ^{69}Ge; $a^r(^{69}\text{Ge}) = a^r(^{75}\text{Ge}) \times \left(\frac{\mu_I}{I}\right)_{^{69}\text{Ge}} \times \left(\frac{I}{\mu_I}\right)_{^{75}\text{Ge}}$

$$= -23.87 \times \left(\frac{0.733}{2.5}\right)\left(\frac{0.5}{0.509}\right)$$

$$= -6.88 \text{ MHz} \quad .$$

C. Calibration Constants Used in the Analysis of the Measurements

$$\mu_o/h = 1.399613 \text{ MHz/G.}$$

$$m_p/m_e = 1836.1$$

^{85}Rb: $g_J = -2.002332$

$$\mu_I = 1.34817 \text{ nm}$$

$$g_I = 2.93700 \times 10^{-4}$$

$\Delta\nu = 3035.7324$ MHz

^{133}Cs: $g_J = -2.002542$

$\mu_I = +2.5641$ nm

$g_I = 3.98994 \times 10^{-4}$

$\Delta\nu = 9192.6318$ MHz.

REFERENCES

[1] A. F. Oluwole, S. G. Schmelling, and H. A. Shugart, Bull. Am. Phys. Soc. 13, 493 (1968); ibid. 13, 1650 (1968).

[2] E. U. Coudon and G. H. Shortley, Theory of Atomic Spectra (Cambridge University Press, London, 1935).

[3] N. F. Ramsey, Molecular Beams (Oxford University Press, 1956).

[4] C. Schwartz, Phys. Rev. 97, 380 (1955).

[5] B. G. Wybourne, Spectroscopic Properties of the Rare Earths (John Wiley & Sons, New York, 1965).

[6] B. R. Judd, Operator Techniques in Atomic Spectroscopy (McGraw-Hill, New York, 1963).

[7] J. C. Hubbs, R. Marrus, W. A. Nierenberg, and J. L. Worcester, Phys. Rev. 109, 3190 (1958).

[8] H. B. J. Casimir, On the Interaction Between Atomic Nuclei and Electrons (Freeman, San Francisco, 1962).

[9] E. Fermi and E. G. Segrè, Z. Physik 82, 793 (1933).

[10] G. Breit and I. I. Rabi, Phys. Rev. 38, 2082 (1931).

[11] H. A. Shugart, Eigenvalue and Least Squares Technique Used by the Atomic Beam Group, LRL (May 1964) (unpublished).

[12] H. Kopfermann, Nuclear Moments (Academic Press, New York, 1958).

[13] P. G. H. Sandars and J. Beck, Proc. Roy. Soc. (London), A289, 97 (1965).

[14] K. Rajnak and B. G. Wybourne, J. Chem. Phys. 41, 565 (1965).

[15] R. M. Sternheimer, Phys. Rev. 95, 736 (1954).

[16] L. S. Goodman and W. J. Childs, Phys. Rev. 141, 140 (1966).

[17] M. G. Mayer and J. H. D. Jensen, Elementary Theory of Nuclear Shell Structure (John Wiley & Sons, New York, 1955).

[18] A. Bohr and B. Mottleson, Dan. Mat.-Fys. Medd. 27, 16 (1953).

[19] L. A. Nordheim, Phys. Rev. 78, 294 (1950).

[20] M. H. Brennan and A. M. Bernstein, Phys. Rev. 120, 927 (1960).

[21] T. Schmidt, Z. Physik 106, 358 (1937).

[22] R. J. Blin-Stoyle, Theories of Nuclear Moments (Oxford University Press, London, 1957).

[23] A. B. Migdal, Nuclear Theory: The Quasi-Particle Method, Translated by A. J. Laslett (W. A. Benjamin, New York, 1968).

[24] O. B. Dabbousi, Nuclear Spins of (45 min) Cs^{125} and (13 day) Cs^{136}; Hyperfine-Structure Separations and Nuclear Magnetic Moments of Cs^{125}, Cs^{136}, and (6.2 hr) Cs^{127}, (Ph.D. Thesis), Lawrence Radiation Laboratory Report (UCRL-16998), July 19, 1966 (unpublished).

[25] C. Moore, Atomic Energy Levels, Vol. II, Circular of the National Bureau of Standards, 467, May 1958.

[26] M. H. Prior, Nuclear Spin and Hyperfine Structure Measurements on the Radioactive Isotopes ^{110}In, ^{121}Sn, and ^{88}Rb, (Ph.D Thesis), Lawrence Radiation Laboratory Report (UCRL-17472), March 25, 1967 (unpublished).

[27] L. S. Goodman and W. J. Childs, Phys. Rev. 131, 245 (1963); ibid. 134, A66 (1964).

[28] C. D. Jeffries, Phys. Rev. 92, 1262 (1953).

[29] R. Trees, Phys. Rev. 92, 308 (1953).

[30] F. D. S. Butement and A. J. Prout, Phil. Mag. 46, 357 (1955).

[31] P. E. Nemivovskii, Nuclear Models (Translated by S. Chomet, Span Limited, London, 1963).

[32] J. K. Temperley, D. K. McDaniels, and D. O. Wells, Phys. Rev. 139B, 1125 (1965).

[33] G. K. Woodgate, Proc. Roy. Soc. (London) A293, 117 (1966).

LEGAL NOTICE

This report was prepared as an account of Government sponsored work. Neither the United States, nor the Commission, nor any person acting on behalf of the Commission:

A. Makes any warranty or representation, expressed or implied, with respect to the accuracy, completeness, or usefulness of the information contained in this report, or that the use of any information, apparatus, method, or process disclosed in this report may not infringe privately owned rights; or

B. Assumes any liabilities with respect to the use of, or for damages resulting from the use of any information, apparatus, method, or process disclosed in this report.

As used in the above, "person acting on behalf of the Commission" includes any employee or contractor of the Commission, or employee of such contractor, to the extent that such employee or contractor of the Commission, or employee of such contractor prepares, disseminates, or provides access to, any information pursuant to his employment or contract with the Commission, or his employment with such contractor.

TECHNICAL INFORMATION DIVISION
LAWRENCE RADIATION LABORATORY
UNIVERSITY OF CALIFORNIA
BERKELEY, CALIFORNIA 94720